DEVELOPMENT OF PARTIALLY STABILIZED ZIRCONIA FOR MAKING CERAMIC BUSHINGS

A Thesis Submitted
in Partial Fulfilment of the Requirements
for the Degree of

MASTER OF TECHNOLOGY

By

NARAYAN CHANDRA BISWAS

to the

INTER DISCIPLINARY PROGRAMME IN MATERIALS SCIENCE

INDIAN INSTITUTE OF TECHNOLOGY KANPUR

JULY, 1980

DEDICATED

TO THE DIVINE SOUL OF MY DEAREST FATHER WHO WAS THE SOURCE OF ALL INSPIRATIONS TO ME.

I PAY TRIBUTES TO MY

DECEASED MOTHER

CERTIFICATE

This is to certify that this work on "Development of Partially stabilized Zirconia for making ceramic bushings" by Narayan Chandra Biswas has been carried out under my supervision and that this has not been submitted elsewhere for a degree.

D Chakravorty

(D. Chakravorty)
Professor
Interdisciplinary Programme of
Materials Science
Indian Institute of Technology,
Kanpur.

ACKNOWLEDGEMENTS

It is a great pleasure to expres my deep and profound sense of gratitude to Dr. D. Chakravarty for his excellent guidence, illuminating suggestions & constant encouragement throughout the course of this work. I enjoyed working with him as freedom of work was available.

I gratefully thank Dr. P.C. Kapoor, Dr. G.S. Murthy, & Dr. A.K. Biswas for their generous permission in allowing me to use their instruments.

I sincerely acknowledge the help rendered by Mr. B. Sharma, Mr. R.K. Prasad, Mr. Malaviya, Mr. J.B. Mukherjee, Mr. Jain, Mr. Pandey (X-ray Lab), Mr. Rahaman in different phases of my work.

I am highly indebted to my friends Messrs A. Sen, G.C. Das, Devendra Kumar, P.K. Das, P. Sarkar, N.K. Ghosh, S. Bhattacharya, D. Kanzilal, Someswar Dutta, Kingshuk Banerjee, Madhukar, N. Dasgupta, S. Chatterjee, Samiran Chattopadhay who have inspired and assisted me throughout the whole journey in various ways.

I am highly thankful to Mr. Ranjit Biswas, Mr. N.L. Mitra, Mr. D. Mukherjee, & Dr. B.N. Samaddar whose financial assistance was the only resort for my admission to IIT, Kanpur.

I am extremely indebted to my mother who departed from us during the Ist semester of my M.Tech, sisters & my brother who patiently beared with the trouble of my absence with understanding and great perseverance when I had to keep myself away from them.

July, 1980 Narayan Chandra Biswas

CONTENTS

LIST OF TABLES

LIST OF FIGURES

SYNOPSIS

The present investigation involved the study of titan addition on Calcia-Zirconia systems in respect to mechanical, thermal and corrosion characteristics. The optimum compositic in respect to bushing material for glass fiber drawing has been searched for. Compositions like 7% (mole) $CaO-ZrO_2$, 10% $CaO-ZrO_2$, 13% $CaO-ZrO_2$, 15% $CaO-ZrO_2$, 8% $MgO-ZrO_2$, 7% CaO- 5% TiO_2-ZrO_2, 8% CaO- 7% TiO_2-ZrO_2, 7% TiO_2-ZrO_2 have been tried using final sintering temperature of 1950°C. Modulus of Rupture, toughness and hardness tests have been done for mechanical characterization.

Titania addition has improved the MOR value and maximum MOR (13, 600 psi) has been obtained for 8% CaO–7% TiO_2-ZrO_2 composition. Toughness has been concluded in term of k_c (stress intensity factor). Slight improvement in k_c value has been found on TiO_2 addition. Highest k_c of 8.75 MN $m^{-3/2}$ has been obtained for 7% TiO_2-ZrO_2 composition.

Vickers hardness value of $CaO-ZrO_2$ and $CaO-TiO_2-ZrO_2$ compositions are comparable. 15% $CaO-ZrO_2$ composition has the highest VPH number.

Spalling characteristics is better for $CaO-TiO_2-ZrO_2$ batches. The composition 7% CaO–5% TiO_2-ZrO_2 is best from the spalling resistance point of view.

Corrosion test has been done on sintered crucibles in contact with E glass for 13 hours at 1400°C. Corrosion resistance is satisfactory for titania-added compositions.

CHAPTER-I

INTRODUCTION

Zirconia is a focus of considerable current interest as an outstanding high temperature oxide outweighing the conventional refractories, as a solid electrolyte, and is a unique field of research in consideration to its stabilization, defect crystallography, toughening and strengthening & electrical transport properties etc.

Because of its very high meeting point (2690°±30°C) (1,2). Very high corrosion resistance to metals, slags and glasses it is used in such applications where temperature and corrosion are very high. Such applications include high temperature extrusion dies, continuous steel pouring nozzles(3), high temperature furnace lining upto 2400°C, lining of furnaces for metting Al, Cr, Co, Au, Ir, Ni, Pd, Pt, Rh metals(4) thermal barrier coatings in air craft and missile components (5), solid electrolyte in fuel cells and steel melts (6), abrasives for melting applications. Glass fibres an usually drawn through bushings made of platinum-rhodium. The high cost of platinum and rhodium makes such process capital-intensive. Recently, ceramic bushings made of alumina as well as stabilised zirconia have been used for making glass fibres (7).

Al_2O_3 is a cheaper material, but does not withstand the corrosive effect of E-glass. Zirconia seems to be a solution to this problem. But zirconia has three polymerphs (2). The stable room temperature form is monoclinic. On heating to about 1100°C it transforms to a tetragonal structure which on further heating above 2300°C transforms to a fluorite type cubic structure. Following the works of Murray, Alison, Wolten, Baily and Patil; Bansal and Heuer (8) have conclusively proved that the monoclinic-tetragonal transformation has all the characteristics of martensitic transformations, i.e. it is of an athermal type, apparently diffusionless & involves a large hysteresis (fig. 1.1) (9). The transformation (forward) on cooling occurs over a much lower temperature range (950-850°C) than the reverse transformation (1100-1190°C) on heating. The monoclinic-tetragonal phase transition renders the material useless as a high temperature structural material, as it is associated with a large volume change (about 9% volume increase on cooling) which cause cracking and subsequent failure of fabricated products. The transformation interval is displaced in the direction of the lower temperature (10) by addition of metallic oxides with a heterapolar bond energy. Thus phase changes may be suppressed by stabilization of the high temperature cubic fluorite form (fig. 1.1) by alloying with

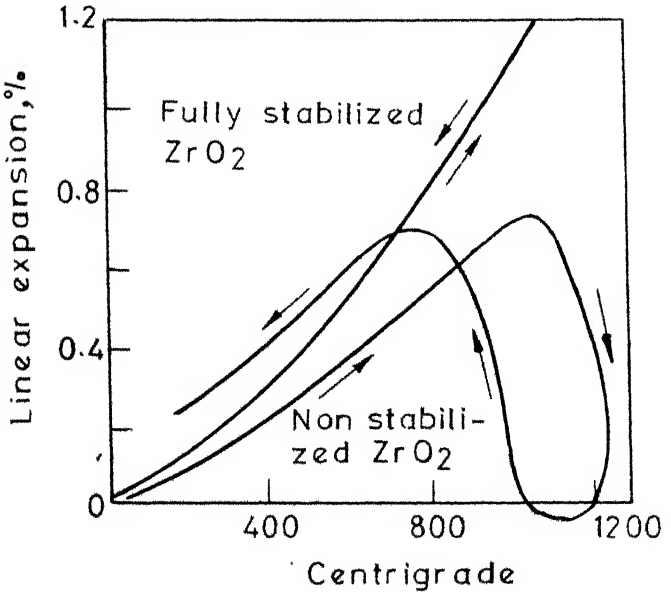

FIG.1-1 THERMAL EXPANSION OF ZIRCONIA MODIFICATIONS (9)

oxides such as those of Mg, Ca, or yttrium. The cubic zirconia solid solution (cubic SS) is infact metastable in all the three systems; alloys of cubic ZrO_2 with MgO, CaO or Y_2O_3. The cubic SS tend to decompose by eutectoid decomposition as predicted from phase equilibria considerations, (fig. 2b). In addition, to the tendency to destabilize, fully stabilized ZrO_2 ceramics have poor thermal shock resistance, because of a combination of low thermal conductivity and high thermal expansion.

It is generally accepted, however, that the most useful mechanical properties are obtained by partial stabilization (11-16) so that a two or three phase microstructure results. These materials are referred to as partially stabilized zirconia (psz). Compositions lying within the cubic field at the firing temperatures and producing monophase microstructure are "fully stabilized" (15).

In recent years, it has been shown that useful mechanical properties of psz, i.e., good fracture toughness and thermal shock resistance can be attributed to a fine dispersion of monoclinic precipitates in the cubic grains (14-15, 17-20). These coherent precipitates are thought to impede crack propagation due to the resulting compressive stresses present in the matrix caused by martensitic

transformation in the particles. The strengthening observed in psz results from crack branching caused by interaction between the stress field of the propagatig crack and residual stress fields around the coherent particles.

If the precipitate size be larger than 2-6 micron, then extensive microcracking takes place due to volume changes on cooling. Because of their large numbers, these cracks propagate only quasistatically and the body maintains a larger portions of its strength after continuous thermal cycling, thus resulting in high thermal shock resistance.

More recently the existence of tetragonal zirconia in sintered bodies with high strength and fracture toughness have been reported (11-13, 16, 21-24). The stabilizing oxides were yttria (11, 25-26), Calcia (16) and Magnesia (21-24).

The reasons of high fracture toughness due to the presence of intragranular tetragonal ZrO_2 precipitates are the following :

1) Initiation of crack is difficult since work has to be done first to cause the phase transformation and then to initiate the crack,

2) The same argument would be true during the

propagation of a crack. As transformation occurs the sudden shape change of the precipitate absorbs strain energy from the crack tip region and a zone of compressive stress is created near the crack tip through which the crack must propagate. Thus, a greater applied stress is necessary for crack growth to continue.

Garvie etal obtained a Ca-psz by a rapid cooling and subsequent ageing treatment. Tetragonal domains which increased in size with time of ageing, were retained at room temperature. The maximum strengthening occured when the tetragonal domains were of a size where they were critically metastable (about 0.1 micron in Ca-psz), i.e. where at room temperature they reverted to a monoclinic form upon the application of mechanical stress.

Similarly, Porter and Heuer have developed 8.1 mole % Mg-psz of optimum mechanical properties, containing homogeneous precipitation of intragranular precipitates. He resorted to special heat treatments of solution annealing of commercial Mg-psz at 1850°C in the cubic SS phase field for 4 hr to dissolve the monoclinic phase present in the as-received material, quenching to less than 1000°C in less than 2 minutes and subsequently ageing between 1400°C and 1500°C, and finally cooling room temperature.

The best materials were those in which the precipitation reaction was nearly two third complete and the precipitates have not lost coherency (size 0.2 mincron in Mg-psz).

Y_2O_3 psz can be obtained routinely at relatively low temperature (less than 1500°C) (11, 26) and the content of tetragonal phase in the polycrystalline ZrO_2 ranged from 98 to 10% Ypsz has the best properties among all the pszs (2, 11, 27), but Y_2O_3 is a very costly rare earth material.

Hannink (2) has claimed to have produced Capsz, Mgpsz, Ypsz by sintering the 9.98 mole % MgO-ZrO_2, 8.4 mole % CaO ZrO_2 and 9.74 mole % Y_2O_3 ZrO_2 followed by solution treatment in the fluorite phase field at 1800°C, cooling to 1300°C, then quenching to 500°C. After natural cooling from 500°C he aged the samples in air. Ageing temperatures were 1400°C for Mgpsz, and 1300°C for Capsz and Ypsz.

Ageing for a long time (over ageing) causes the tetragonal particles to grow beyond critical size (0.1 micron for Capsz, 0.2 micron for Mgpsz and 0.3 micron for Ypsz depending on the composition). These particles lose coherency with the matrix and transform readily to monoclinic symmetry when cooled.

ZrO_2-TiO_2 system has been investigated by several

workers in early 50's but was not thoroughly studied afterwards. The phase diagram by Duwez, Brown and Odell (9) (fig. 2d) shows that the addition of TiO_2 to ZrO_2 causes a rapid decrease of both liquidus and solidus curves, from 2715 to 1820°C, the latter is the incongruent melting temperature of $ZrTiO_4$.

The addition of TiO_2 also lowers the transformation temperature of zirconia from 1000°C to approximately 350°C. However, stabilization, i.e. formation of cubic phase does not take place.

Voromin (28) has shown that addition of 1% TiO_2, to stabilized zirconia increases the compressive strength from 1050 Kg/cm^2 to 1450 Kg/cm^2. Further increase to 2% decreases the strength to 500 Kg/cm^2. Further addition of TiO_2 increases the compressive strength and at 5% the strength is about as original.

By going to explore the feasibility of making inexpensive electrolytes using the tape process, Radford & Bartton (1976)(6) has added 5 mole % TiO_2 to commercially stabilized zirconia (5 wt % Ca sz & 12 wt % Y_2O_3 sz) so that the tape along with the electrode material, platinum could be sintered to impervious, high density (93%) electrolyte by sintering at 1500°C.

Coughanaur (29) has observed the existence of a single phase solid solution in the ZrO_2 rich corner of the CaO-TiO_2-ZrO_2 phase diagram (fig. 2.e).

The ionic radii of Ca^{2+}, Mg^{2+}, Y^{3+}, Ti^{4+} and Zr^{4+} are shown below (30).

Species	Ca^{+2}	Mg^{+2}	Y^{+3}	Zr^{+4}	Fe^{+3}	Ti^{+4}
Atomic number	20	12	39	40	26	70
Atomic radii	1.969	1.594	1.79	1.58	1.241	1.458
Ionic radii (30)	1.06	0.78	1.06	0.87	0.67	0.64
Crystal structure	Fcc	Hex		Hcp	Bcc	Hcp
Ionic radii, (Pauling)	0.99	0.65	0.93	0.80		0.68

The average ionic radius of Ca^{2+} & Ti^{4+} is 0.85 aungstrom, close to that of Zr^{4+}. So it is likely to form a solid solution of CaO-TiO_2-ZrO_2.

It seems probable that compositions containing smaller percentages of CaO than is required to fully stabilize the ZrO_2 and some amount of TiO_2 would produce a psz which can retain tetragonal precipitates due to lower tetragonal monoclinic inversion temperature and would have a high fracture toughness, strength and thermal shock resistance.

With the problem of low thermal shock resistance of the glass fiber drawing bushings in view and the above

intension the present study was aimed at improving these thermal and mechanical properties without resorting to any quenching operation.

CHAPTER-II

OBJECTIVES OF INVESTIGATION

(1) To develop partially stabilized zirconia (psz) of high strength, corrosion resistance and thermal shock (spalling) resistance by addition of ($CaO+TiO_2$).

(2) To find optimum composition for CaO.psz.

(3) To study whether TiO_2 stabilizes ZrO_2 or not.

(4) To study the stabilization & properties of stabilised zirconia from indigenous monoclinic ZrO_2.

(5) X-ray diffraction studies on the stabilized & partially stabilized zirconia to identify the different phases present (estimate their percentages).

(6) Comparison of thermal shock resistance of the stabz & pszs.

(7) To study the corrosion by E-glass on the stabz, pszs & Al_2O_3.

(8) Measurement of modulus of rupture in bending for the psz and stab Z's.

(9) Measurement of hardness and stress intensity factor of the pszs and stabzs.

(10) Determination of apparent porosity, true porosity and bulk density of slip cast crucibles and pressed samples. Determination of true density, true porosity and closed porosity of pressed samples.

(11) Optical microscope studies on stabz and pszs samples after thermal shock resistance test.

(12) X-ray diffraction studies to estimate the changes in phase composition during thermal shock resistance test.

CHAPTER-III

EXPERIMENTAL PROCEDURE

3.1 Raw Materials

Monoclinic Zirconia from Indian Rare Earths Ltd., and $CaCO_3$, TiO_2, MgO of Laboratory reagent grade were used. For comparison, imported commercial stabilized zirconia, ZircoaB, manufactured by Corhart Refractories Co., U.S.A. was also used to make crucibles and plates.

3.2 Sample preparation

3.2.1 Weighing & Mixing :

Monoclinic zirconia was weighed on a pan balance. $CaCO_3$, TiO_2 & MgO were weighed in a chemical balance. The different batches with different additives were dry-mixed in a ball mill for 2 hrs. for each batch. The compositions are shown in table 3.1.

3.2.2 Precalcination :

The batches were mixed with water and some irregular shapes were made by hand. The batches were precalcined at 1200-1300°C in order to

a) remove CO_2 from the batches carrying $CaCO_3$,

b) reduce size, c) facilitate handling.

TABLE 3.1

BATCH COMPOSITIONS

Batch	ZrO_2 mole %	CaO mole %	TiO_2 mole %	MgO mole %
C7	93	7	-	-
C10	90	10	-	-
C13	87	13	-	-
C15	85	15	-	-
C7T5	88	7	5	-
C8T7	87	8	7	-
T7	93	-	7	-
Stab Z (Commercial Zircoa B)	Unknown	-	-	-
M8	92	-	-	8

3.2.3 Calcination

The batches were calcined in a zirconia lined furnace (fig. 3.3) by Indane-Oxygen gas firing. The temperature was raised to 1850°C in 5-6 hrs, & then the temperature was maintained for 4 hrs. The M8 batch was calcined at 1350°C in a globar furnace.

3.2.4 Crushing

Primary crushing of calcined lumps were done in the jaw crusher, and then secondary crushing was done in the roll crusher. The particles were reduced to a maximum size of 2 mm. The iron rust particles which came in during crushing were sorted out by a magnet.

3.2.5 Grinding

Grinding was done in a high alumina porcelain lined ball mill with alumina balls using water as the liquid. Some batches were ground in a agate centrifugal ball mill (Pulverizetle, Fritsch, Germany, Type 05.102) also. The grinding that has been done for different batches is shown in Table 3.2.

The C7T5 and C8T7 batches were ground for a longer time since these developed poor casting properties i.e., quick settling property after 82 hrs of grinding.

TABLE 3.2

GRINDING HOURS

Batch	Hours of grinding		
	in Alumina ball mill	Agate Centrifugal ball mill	Chart speed
C10	90	-	-
C13	82	-	
C7	37	35	5
C15	-	50	6
C7T5	106	-	
C8T7	106		
T7	18		
M8	20		

The batch T7 was weak and crumbly, so a shorter period of grinding was given to the batch. The M8 batch was calcined at 1350°C and so it was ground for a short time.

3.2.6 Sieving and Magnetic Separation

The slip produced on grinding were passed through a 325 mesh ASTM sieve. Some of the batches were dried and granulated. Then magnetic separation was tried for in a magnetic separator but the efficiency of separation was poor.

Finally magnetic separation was done by keeping two Alimco bar magnets in the slip kept in a plastic bucket and stirring the slip by a 3 blade stirrer. The magnetic particles adhering to the edges and corners of the magnets were wiped out from time to time at 10-15 minutes interval by cotton. This process was continued till insiginficantly small amount of magnetic particles got adhered to the magnet over a long time interval.

3.2.7 Preparation of Plaster of Paris Moulds

A wooden model was cleaned and brushed with soap solution. Then it was oiled with coconut oil by a brush. The model was enclosed in a thick sheet of paper folded into a cyclindrical form and was bound with threads. The plaster of paris slip was poured on to the model and it was allowed to set for ~ 30 minutes after which the mould was released from the model. Several moulds (fig. 3.4) were made in this way.

3.2.8 Slip Casting

Slip casting was done for all the batches. The C8T7 batch settled very quickly and a small amount of Na_2CO_3 (~ 0.1%) was added before slip casting whereby the casting properties improved. The T7 batch also settled very quickly

but casting was done without any addition.

3.2.9 Pressing

Pressing was done in a hydraulic press with a pressure of 14.2 KN/cm^2 (20610 psi).

The powder was mixed throughly with 2% PVA solution in a quantity to have proper pressing characteristics, i.e., easy mould release, proper compaction, avoidance of extra water release during pressing and avoiding crumbliness of the pressed sample. The moist powder was put in the high chromium high carbon alloy steel mould (fig. 3.1) - having an inner dimension of 5 cm x 1 cm x 1 cm. It was levelled by the punch. Then the mould with the punch was kept on the platform of the hydraulic press. Pressure was applied at a slow rate (in ~ 2 minutes). After attainment of the maximum load, 2 minutes were allowed before the release of the pressure in order to homogenize the pressure distribution. The sample was released in a hydraulic hand press.

The percentage of water added was determined on the dry basis and are shown in the table.3.3 below.

Table 3.3 Water of Granulation for Pressing

Batch	Water % on dry basis	Batch	Water % on dry basis
C7T5	9-11	C15 C15	4.3-4.5
C7	6.4-7	T7	6.7-7.3
C10	4.9-5	M8	3.2-4

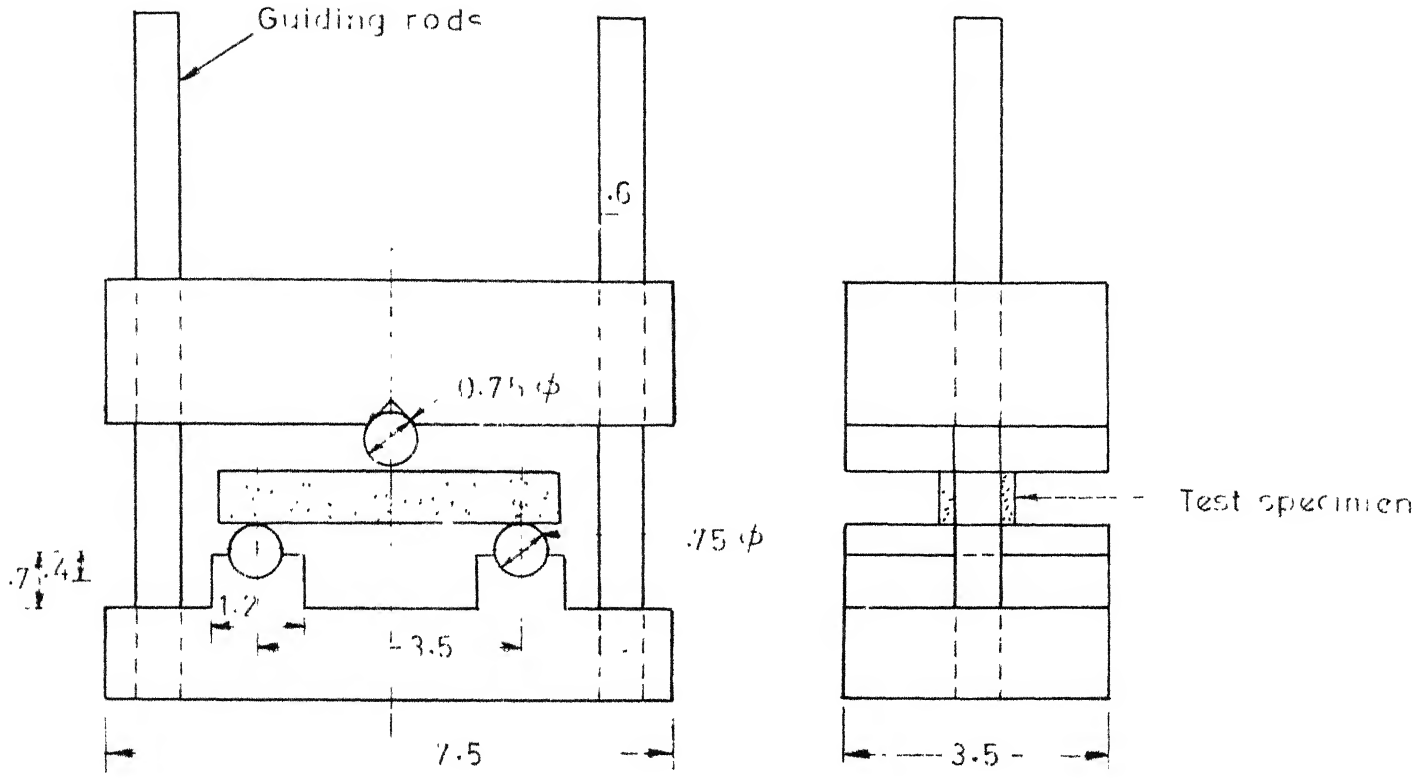

FIG. 3·2 FRONT VIEW AND SIDE VIEW OF THE BEARING EDGES FOR MODULUS OF RUPTURE TEST

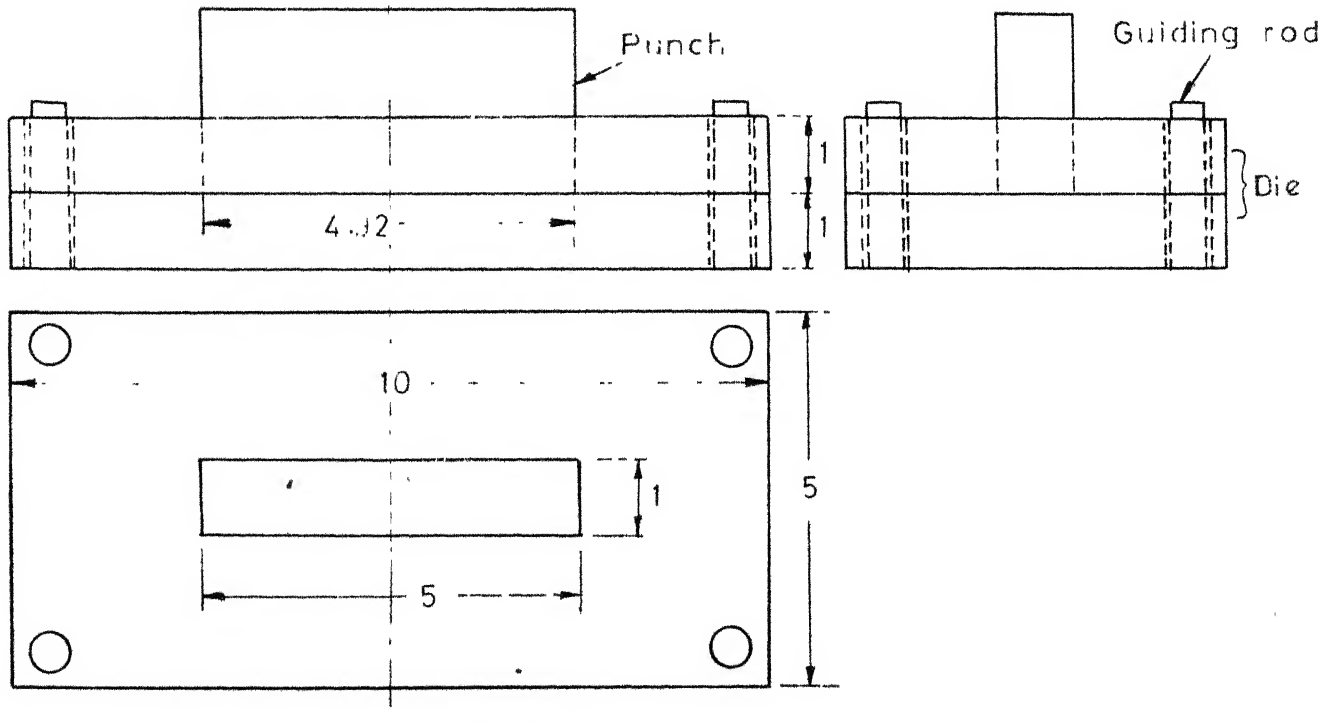

FIG. 3·1 DESIGN OF THE MOULD ASSEMBLY USED FOR PRESSING.

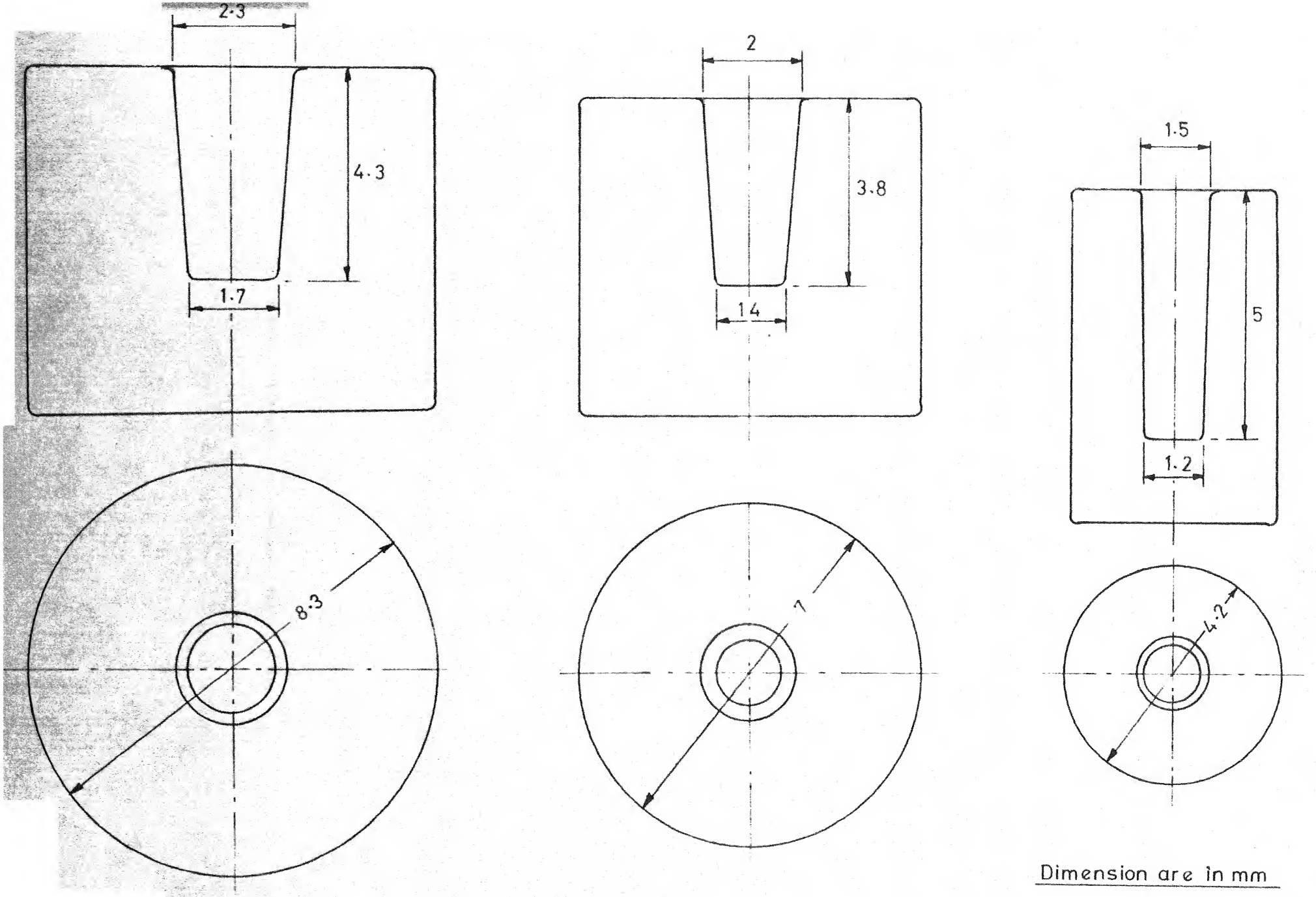

FIG.3.3 PLASTER OF PARIS MOLDS USED FOR SLIP CASTING.

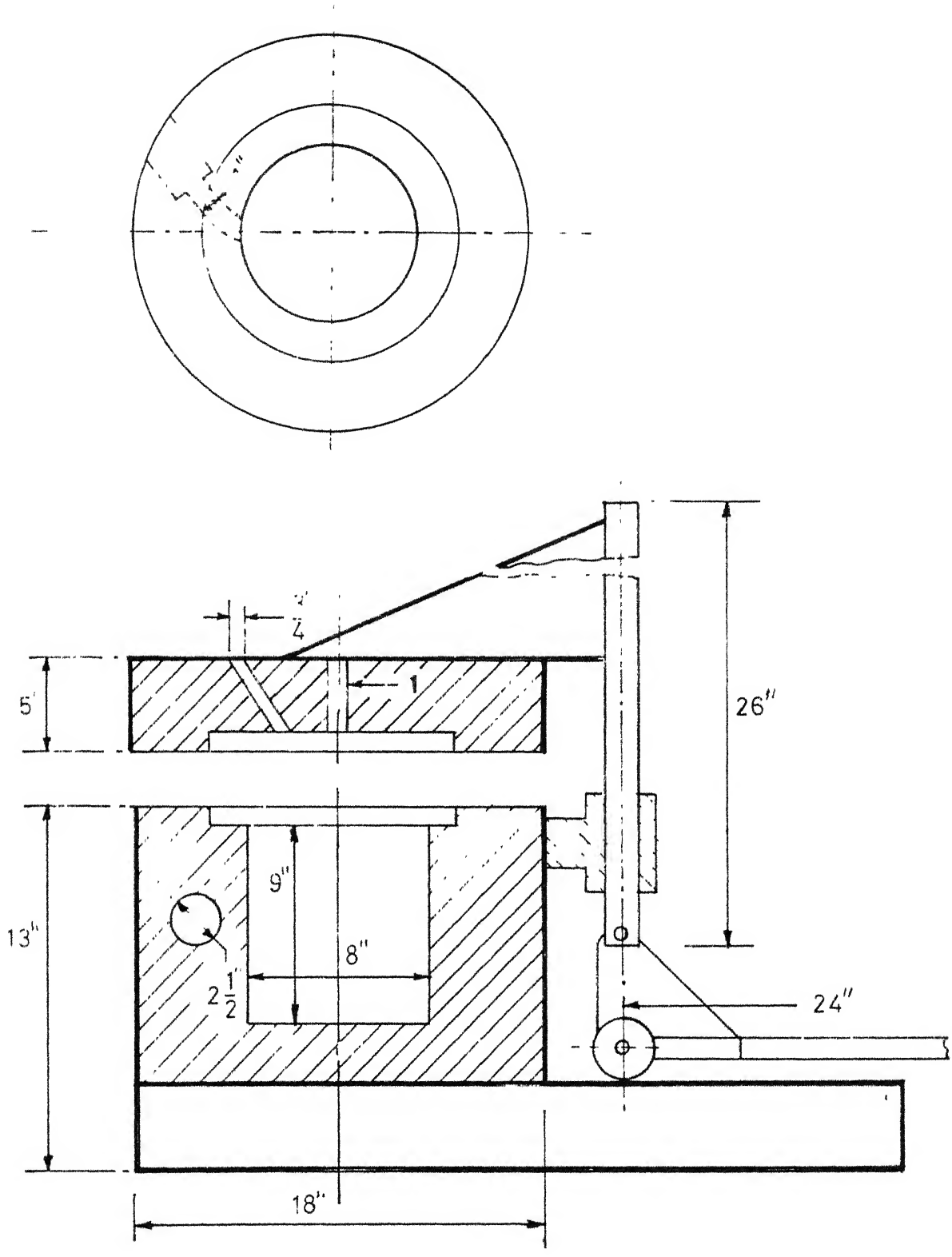

FIG. 3.4 ZIRCONIA LINED FURNACE

3.2.10 Drying

The slip cast crucible were air dried and the pressed samples were dried in an oven at 180°C.

3.2.11 Presintering and finishing

The crucibles were presintered at 800°C in an annealing furnace for 5 hrs. The rims were polished by rubbing on a plain paper.

3.2.12 Sintering

The test bars and crucibles were set in the zirconia lined furnace (fig. 3.3). Indane-oxygen gas firing was used. Temperature was raised to 1950°C in 14 hours and soaking of 1 hr was given at that temperature. The temperature was reduced to 1350°C in 12 hrs and then the gas firing was shut off, and the furnace allowed to cool by itself.

3.3 X-ray Diffraction Studies

Solid bars of the sintered samples and samples after thermal shock resistance test were mounted on the X-ray diffractometer. The operational variables are listed in table 3.4. The angles at which well derined peaks appeared were noted down and the corresponding 'd' values were calculated from the Bragg equation,

$$n\lambda = 2d \sin \theta \quad \ldots\ldots\ldots (3.1)$$

TABLE 3.4

PARAMETERS USED IN X-RAY DIFFRACTOMETER

Radiation used	:	CuK, ... (= 1.5405 Å)
Filter	:	Ni
Voltage rating	:	35 KV
Current	:	12 mA
Intensity range	:	1000 counts per second
Time constant	:	2 seconds
Beam slit	:	3°
Detector slit	:	0.2°
Scan speed	:	2° per minute
Chart Speed	:	2° per minute
Speed controlling disc	:	C

where n = an integer, taken as 1. = wave length of X-ray radiation, Θ = Bragg angle, d = inter planar spacing.

The 'd' values & the relative intensities from peak heights were compared with the standard powder diffraction file (PDF) in order to identify the crystalline phases. the integrated area of the 100I peaks of different phases were determined by trapezium method by using the following equation (3.2),

$$\text{Area, } A = h. \left[\frac{f_1}{2} + f_2 + f_3 + f_4 + \ldots\ldots \frac{f_{n+1}}{2} \right] \quad \ldots(3.2)$$

where h = length of one division

n = number of divisions

and f_1, f_2, f_3 ....., f_{n+1} are the respective functions at the divisions, 0, 1, 2, ... n.

The phase analysis was done according to the modified formula in polymorphsmethod developed by Garvie & Nicholson Volume fraction of monoclinic phase,

$$V_m = \frac{1.603 \left[I(11\bar{1})m \right]}{1.603 \left[I(11\bar{1})m + I(111)c \right]} \quad \ldots\ldots(3.3)$$

where $I\ (11\bar{1})_m$ = integrated intensity of the $(11\bar{1})$ monoclinic reflection.

$I(111)_c$ = integrated intensity of the (111) cubic reflection and it is assumed that

$$V_m + V_c = 1 \quad \ldots\ldots(3.4)$$

V_c = Volume fraction of cubic phase

V_m = Volume fraction of monoclinic phase.

3.4 Thermal Shock Resistance (Spalling resistance) Test

A globar furnace with thick SiC rods as heating elements and high duty fireclay lining was used for the test. The furnace can regain the temperature drop during removal of the samples in about 10 minutes. The rectangular bar test pieces were kept in a refractory support and placed inside the furnace. The furnace was heated at a uniform rate so that 1300°C was attained in 4 hrs. The temperature was maintained for 30 minutes and then the support containing the samples was removed from the furnace with large tongs. The samples were placed on a brick in a position free from draughts. After they had been cooled for 10 minutes they were examined and then replaced into the furnace for a further period of 10 minutes. Then the cycle was repeated. The test was concluded when the specimens could be pulled apart by light tongs. One highduty insulation brick support could be used for two cycles.

3.5 Corrosion Resistance Test

The E glass marbles were melted in a sillimanite crucible and quenched into water to get small particles of

the glass. The crucibles were filled with the E glass and put on the grooves made by drilling in a highduty insulation brick support. The support with the crucibles was kept in the globar furnace and heated to 1400°C in 8 hrs. The temperature was maintained for 13 hrs. Then the furnace was cooled down to room temperature. The bottoms of the crucibles were cut into two vertical cross sections by diamond tipped wheel. The two sections were broken apart by a small hammer. Photographs of the cross sections of the crucibles were taken and corrosion of the crucibles were studied.

3.6 Determination of apparent porosity, apparent (bulk) density, true porosity & true density. (32)

3.6.1 Apparent porosity & bulk density.

The test specimens were dried at 110°C and weighed (W) after cooling to room temperature in a desiccator. The test specimens were placed in distilled water and boiled for about 2 hrs. then these were allowed to cool to room temperature, while still immersed in water. The test specimen was weighed while suspended in water (W_2). Immediately after obtaining the suspended mass, the test specimen was removed from water, blotted lighly with a wet tissue paper and weighed in air (W_1).

Then apparent porosity & apparent density were calculated from the following formulae :

Apparent (bulk) density, $D_A = \frac{W}{W_1 - W_2}$ .....(3.5)

Apparent porosity, $P_A = \frac{W_1 - W}{W_1 - W_2} \times 100$ .....(3.6)

3.6.2 True Specific gravity, true density and porosity

3.6.2.1 Sample Preparation

Samples weighing about 20 gms were ground in an to such a fineness that they would pass through 149-micron IS-Sieve. The sample was dried at 105 to 110°C.

3.6.2.2 The pycnometer was washed, dried and weighed (P). About 4 to 6 gms of sample was placed in the dry pycnometer and weight of pycnometer, stopper plus sample (W) was taken.

The pycnometer was filled to one-half of its capacity with distilled water which had been boiled to remove dissolved air and cooled. The pycnometer was kept on a hot plate to boil the water for 10 to 15 minutes. Then the pycnometer was kept in a distilled water bath in a glass petri-dish to cool the pycnometer to room temperature. The pychometer was filled with water, the stopper was inserted and the excess water was wiped off from the stopper. The

pycnometer was throughly dried with a tissue paper. Then pychometer & the contents were weighed (W_2). The sample was thrown away, the pycnometer was washed and filled with water, and it was weighed after drying the outside with tissue paper.

The specific gravity, true density and true porosity were calculated from the following formulae :

$$\text{Specific gravity, } S = \frac{W - P}{(W-P) - (W_2-W_1)} \qquad \ldots\ldots(3.7)$$

where

W = mass in gm of the stoppered pycnometer and sample.

P = mass in gm of the stoppered pycnometer

W_2= mass in gm of the stoppered pychometer, sample and water.

W_1= mass in gm. of the stoppered pycnometer filled with water.

$$\text{True density} = \text{Sp. gr.} \times (d_w - d_a)$$

where d_w = density of water at the temperature at which the test was carried out, and

d_a = density of air at the temperature at which the test was made.

$$\text{True porosity, } P_T = 1 - \frac{\text{Apparent density, } D_A}{\text{True density, } D_T} \qquad \ldots\ldots(3.8)$$

$$\text{True porrosity, percent} = \left(1 - \frac{D_A}{D_T}\right) \times 100 \qquad \ldots\ldots(3.9)\ (32)$$

$$\text{Closed porosity } P_C \text{ (percent)} = P_T\ (\%) - P_A(\%) \qquad \ldots\ldots(3.10)$$

3.7 Microstructural Studies by Optical Microscopy

3.7.1 Sample Preparation

The samples were joined together into two batches by quick fix in order to polish a few samples together. These were polished with Sic Powders of mesh sizes 220, 400, 600 and 800 successively. After this optical polishing was done on a polishing wheel with diamond paste. Little amount of liquid paraffin was added to the diamond paste and also added again for 2-3 times during polishing. Final polishing was done with 0.3 micron and 0.05 micron Al_2O_3 powders successively to remove the pits in the sample produced during polishing by diamond paste.

3.7.2 Microstructure

Photographs were taken with the microscope focussed at a magnification of 200X and 400X for sintered samples and 400X for the spalled samples. Camera magnification was 1/3rd the microscope magnification. An exposure time of 3 seconds was given in each case. The photographs after enlargement during printing were studied for different phases, grain structure and changes on spalling (thermal shock).

3.8 Particle size analysis of the ground batches

Different solvents were tried to disperse the particles and a mixture of Ethyl alcohol, methyl alcohol and acetone was found to be the best. The mixed solvent was taken in an agate mortar in small amount. A pinch of the powder was added to it. It was mixed with the liquid by whirling the paste. Then the mortar with the contents was placed in the water bath of an ultrasonic cleaner and the bath was vibrated with ultrasonic waves for ten minutes. Immediately after this one or two drops of suspension were dropped on a cleaned glass slide with the help of a dropper and allowed to spread and dry in air.

The slide was kept in a petri dish. The photograph of the particles were taken with 400 X magnification in the microscope, combined with the 3 times reduction by the camera. Printing of the photographs was done with an enlargement of 3.5. Each photograph of different batches was divided into several areas and the size of the particles of each area was read by a scale. The number of particles in different size ranges were obtained and particle size distribution was thereby found out.

3.9 Modulus of rupture

The sintered bars were ground with 220 mesh SiC powder to give proper rectangular shape and an approximate dimension of4-4.5 x .9 x .7 cm. The samples were polished with SiC powders of mesh sizes 400, 600 and 800 successively.

The samples were tested in the Instron machine with the bearing Edges for modulus of rupture test, shown in figure (3.2).

The load cell used had a range of 0-200 Kgs with a least count of 2 Kg. The cross head speed used was 0.2 mm/min. Chart speeds of 0 cm, 2-0 cm, 5 cm per minute were used.

The Instron was first calibrated to read 200 Kg in the full span of the chart.

The sample was mounted on the bearing edges of the Modulus of rupture test jig (fig. 3.2) kept on the platform of the Instron under the cross head.

The load was applied by downward movement of the cross head. The maximum atbreaking load after which the specimen failed suddenly was obtained from the chart.

From the breaking load, the modulus of rupture was calculated from the following formula :-

$$\text{Modulus of Rupture, in Kgf/cm}^2 = \frac{3Wl}{2bd^2} \qquad \ldots\ldots(3.11)$$

where, W = load in Kgf at which the specimen failed,

l = distance in cm between the centre lines of the lower bearing edges,

b = width of the specimen in cm, and

d = depth of specimen in cm.

3.10. Vickers Hardness and Fracture toughness

The hardness was measured by indenting polished samples using a square base diamond pyramid as indentator (33) in the vickers pyramid hardness testing machine (Vickers Instruments Ltd., England, model No. 255038).

Because of the shape of the indenter this is frequently called the diamond pyramid hardness test. The diamond pyramid hardness (DPH) or Vickers hardness number (VHN or DPH) is defined as the load divided by the surface area of the indentation.

$$DPH = \frac{2P \sin(\theta/2)}{L^2} = \frac{1.854\ P}{L^2} \qquad .....(3.12)$$

where P = applied load, Kg.

L = average length of the diagonals, mm.

θ = angle between opposite faces of diamond = 136°.

The fracture toughness was determined by a technique developed by Evans & Charles (34) using the dimensional analysis of indentation crack length (c) and impression

radius (a).

Fracture toughness, k_c is obtained from the following formula :-

$$k_c \phi/H\sqrt{a} = 0.15\ k\ (\frac{c}{a})^{-3/2} \quad \ldots.(3.13)$$

where k_c = fracture toughness

ϕ = the constraint factor (~ 3)

H = hardness

a = impression radius

c = crack length

k = a correction factor

The function $\frac{k_c}{H\sqrt{a}} \left[\frac{H}{E\phi} \right]^{0.4}$ when plotted with $\frac{c}{a}$, produces a unique curve which fits for all the polycrystalline materials. The straightline curve for single crystals fall close to those of polycrystals.

The samples which were used for studying the microstructure were taken. Opposite surface to the polished one was ground in 220 mesh SiC powder to make the two surfaces parallel. In the vickers hardness testing machine loads of 2.5 kg and 5 kg and were used for the test. For each load several indentations were made. In each case the diagonal of the indentation, the average crack length of the cracks produced by indentation were measured by ocular reading, oneocular reading corresponds to

0.001 mm.

Hardness corresponding to each reading was read off the vickers chart. Hardness values in Nm^{-2} unit was also calculated from equation (3.9) for use in determining k_c.

Using the measured impression radius, cracklength and hardness, the fracture toughness was determined from the calibration curve (34, 13).

Photographs of some of the indentations were taken.

CHAPTER-IV

RESULTS AND DISCUSSION

4.0 Particle Size analysis

The results of the particle size analysis of the ground ZrO_2 powder before shaping are shown in table 4.1. The particle size distributions are shown in the figures 4.1, 4.2, and 4.3.

All the batches have highest distribution density at less than or equal to 0.214 micron size. The maximum particle size observed is 3.65 micron. So the powders are very fine. This is because of the fact that the batches have been ground for a very long time in order to develop good casting properties.

4.1 Densities and porosities

The bulk density, true density, apparent porosity, true porosity and closed porosity values of the different batches are recorded in table 4.2, and 4.3. The variation of true density and true porosity values as a function of composition are shown in figures 4.4 and 4.5 respectively for sintered bars made by pressing and figures 4.6, 4.7 for crucibles made by casting. The bulk density is much less than the true density and most of the porosity is due to

TABLE 4.1

PARTICLE SIZE ANALYSIS OF THE GROUND BATCHES

Size range, micron	No. of Particles falling in the size range for batches								
	C7	C10	C13	C15	C7T5	C8T7	T7	Stabz	M8
< 0.214	35	30	56	19	43	32	73	63	126
0.214– 0.429	21	20	16	23	25	27	28	57	96
0.429– 0.643	15	7	4	16	17	13	17	29	53
0.643– 0.857	4	4	2	3	16	3	27	11	15
0.857– 1.072	4	4	3	4	3	4	26	7	9
1.072– 1.286	1	1	3	2	1	4	20	9	7
1.286– 1.499	3	2	9	–	3	2	11	6	4
1.499– 1.714	5	5	7	1	1	4	18	5	3
1.714– 1.929	1	1	5	2	1	–	11	4	1
1.929– 2.143	5	4	4	6	2	2	19	11	2
2.143– 2.357	3	4	1	5	2	–	–	5	–
2.357– 2.571	8	6	2	9	1	1	11	5	–
2.571– 2.786	3	3	2	1	–	1	–	3	–
2.786– 2.999	1	–	3	1	–	1	7	1	1
2.999– 3.214	2	2	2	2	–	–	1	–	–
3.214– 3.429	–	–	4	–	–	–	–	–	–
– 4.286	–	–	–	1	–	1	–	–	–

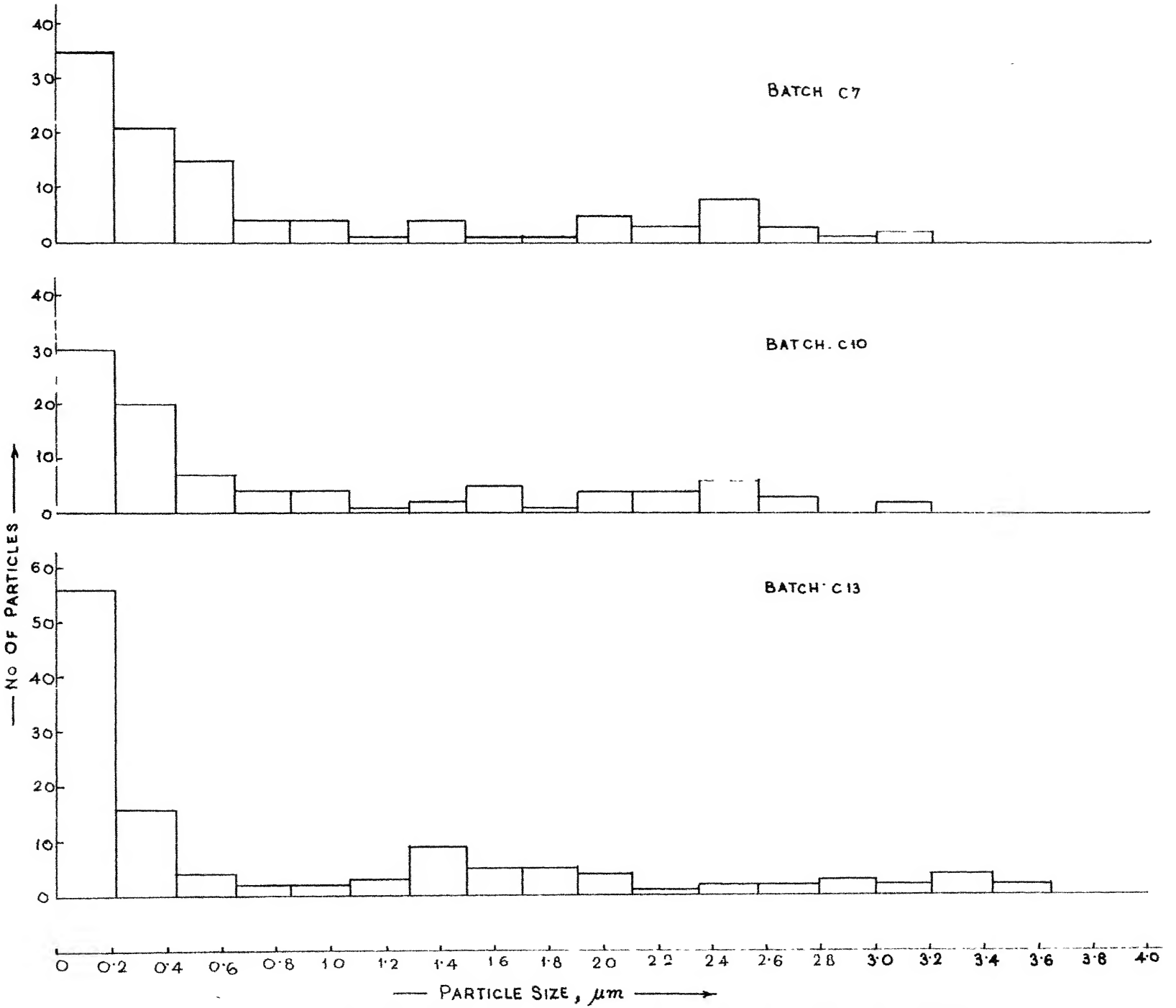

FIG. 4·1 PARTICLE SIZE DISTRIBUTION OF GROUND ZIRCONIA BATCHES.

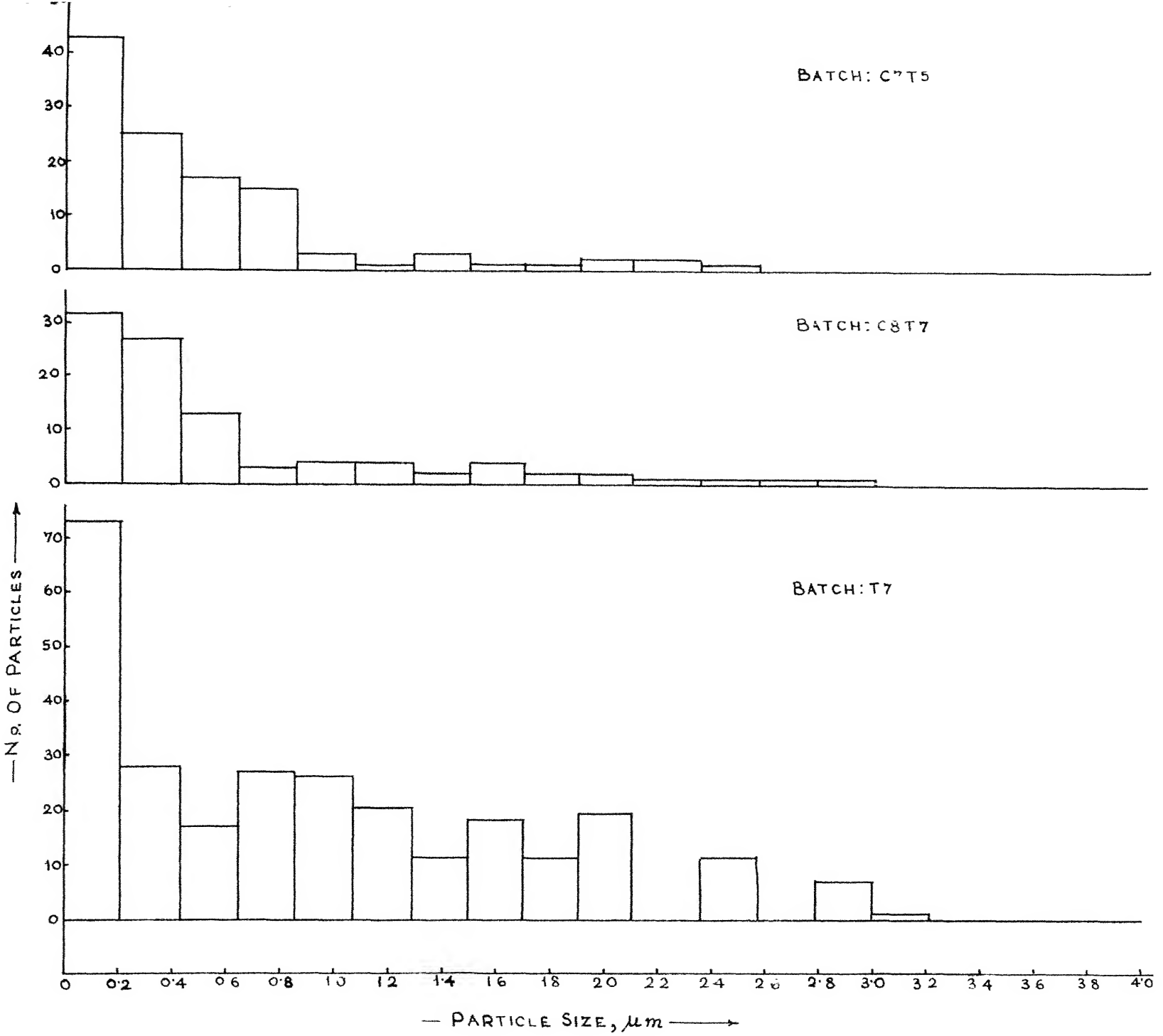

FIG 4·2 PARTICLE SIZE DISTRIBUTION OF GROUND ZIRCONIA BATCHES.

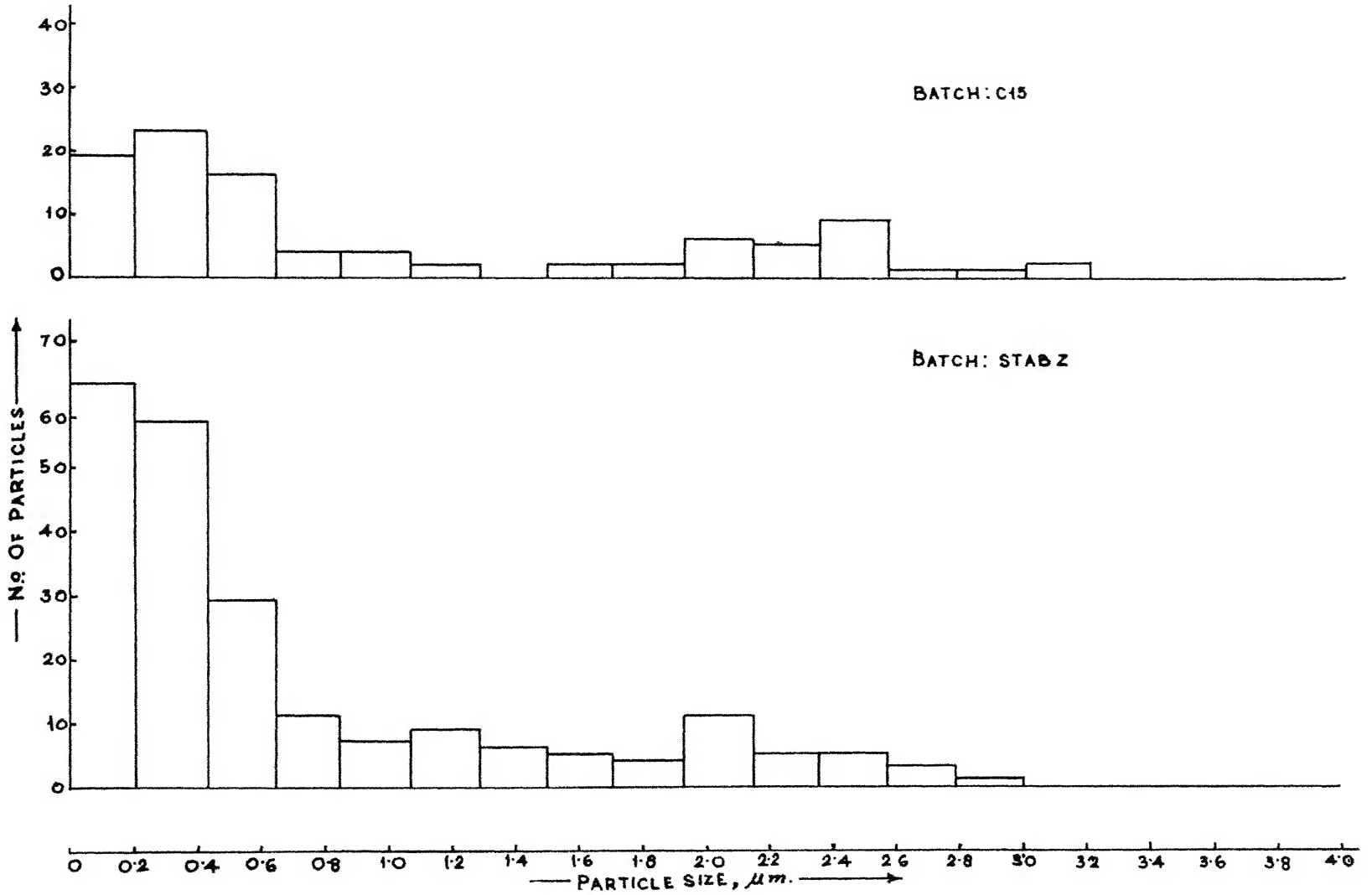

FIG. 4·3 PARTICLE SIZE DISTRIBUTION OF GROUND ZIRCONIA BATCHES.

TABLE 4.2

TRUE DENSITY, BULK DENSITY, APPARENT, CLOSED AND TRUE POROSITIES OF THE SINTERED SAMPLES

Sintered bars	True density D_T, gms/cc	Bulk density D_B, gms/cc	Apparent porosity P_A %	Closed porosity P_C %	True porosity P_T %
C7	5.364	4.794	1.076	9.554	10.63
C10	5.373	5.083	1.910	3.429	5.399
C13	5.404	5.133	1.620	3.404	5.006
C15	5.572	5.300	0.000	4.115	4.115
C7T5	5.475	4.730	1.457	12.153	13.610
C8T7	5.541	4.822	1.603	11.377	12.980
T7	5.486	4.733	1.020	12.703	13.723
M8	5.246	4.320	3.730	13.921	17.651

TABLE 4.3

APPARENT DENSITY, BULK DENSITY, APPARENT CLOSED AND TRUE POROSITIES OF THE CRUCIBLES

Crucibles	Bulk density D_B gms/cc	Apparent porosity P_A %	True porosity P_T %	Closed porosity P_C %
C7	4.914	6.946	8.380	1.434
C10	5.038	1.665	6.237	4.572
C13	5.153	1.715	4.631	2.916
C15	5.370	0.000	3.625	3.625
C7T5	4.882	2.785	10.830	8.045
C8T7	5.101	2.126	7.930	5.810
T7	4.998	3.354	8.892	5.538
M8	4.642	7.300	11.514	7.300
Stab z	5.062	2.926	8.562	5.636

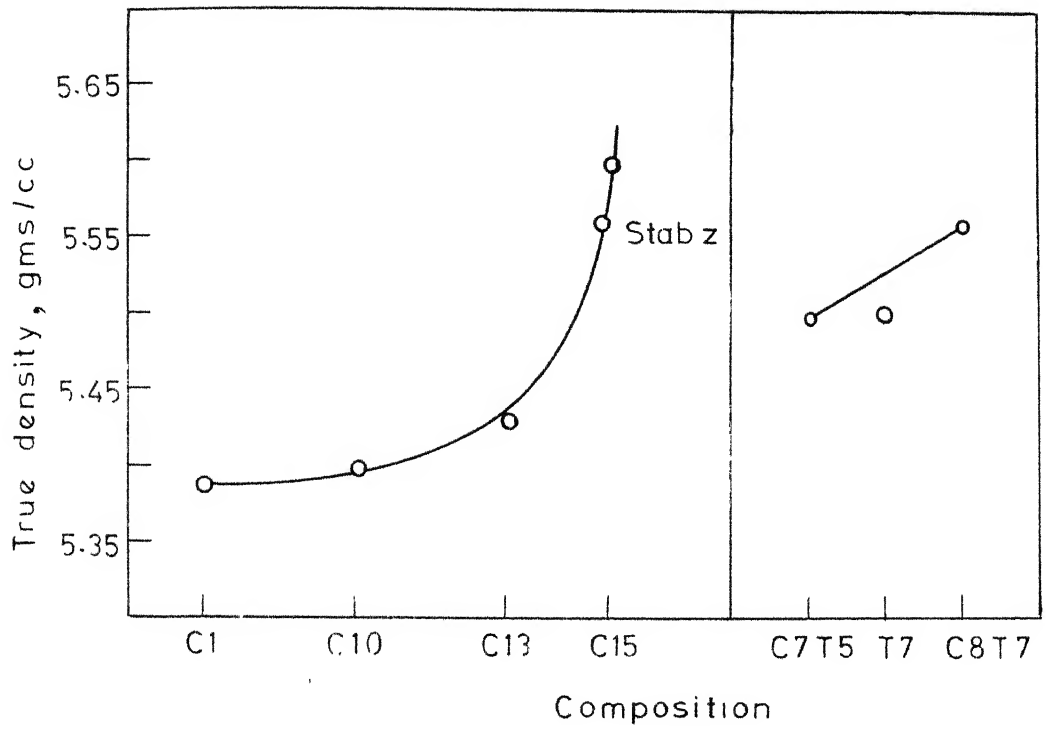

FIG. 4.4 TRUE DENSITY VS. COMPOSITION

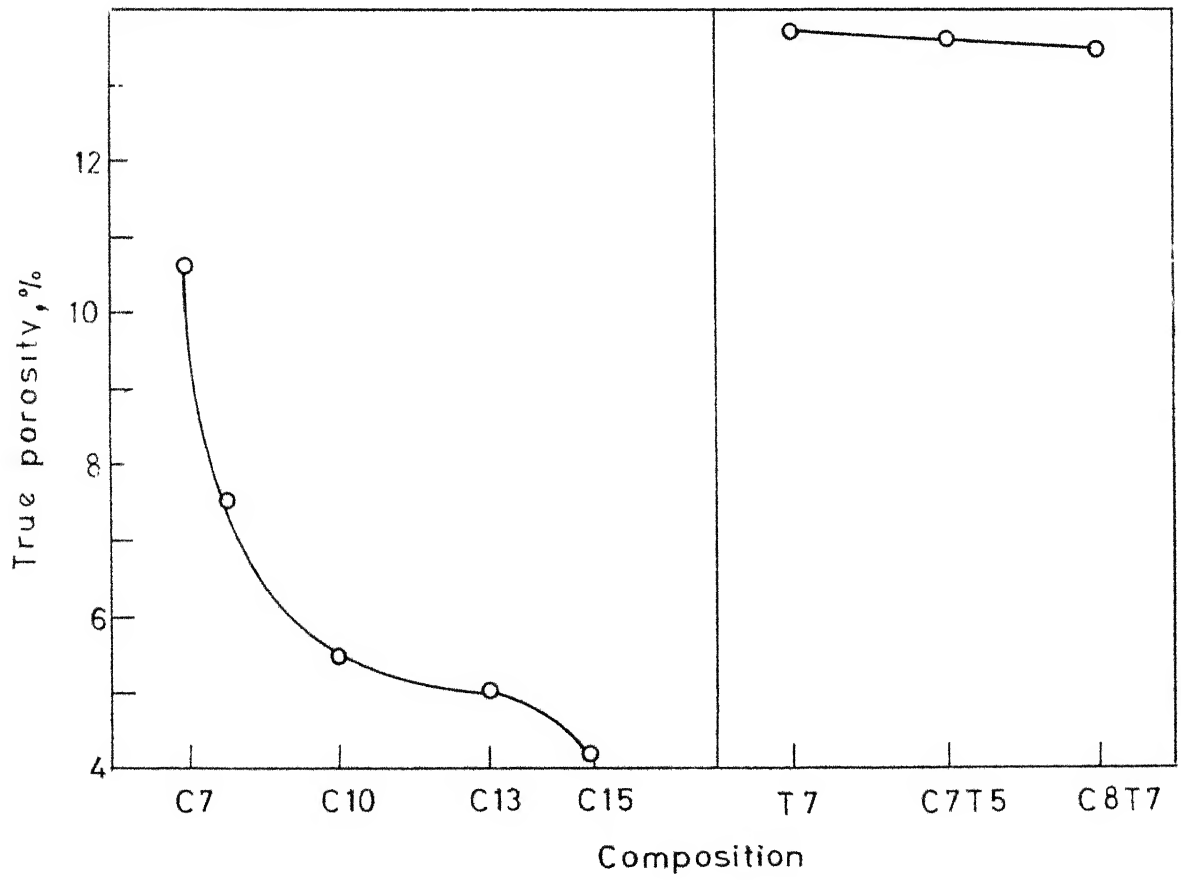

FIG. 4.5 TRUE POROSITY VS. COMPOSITION

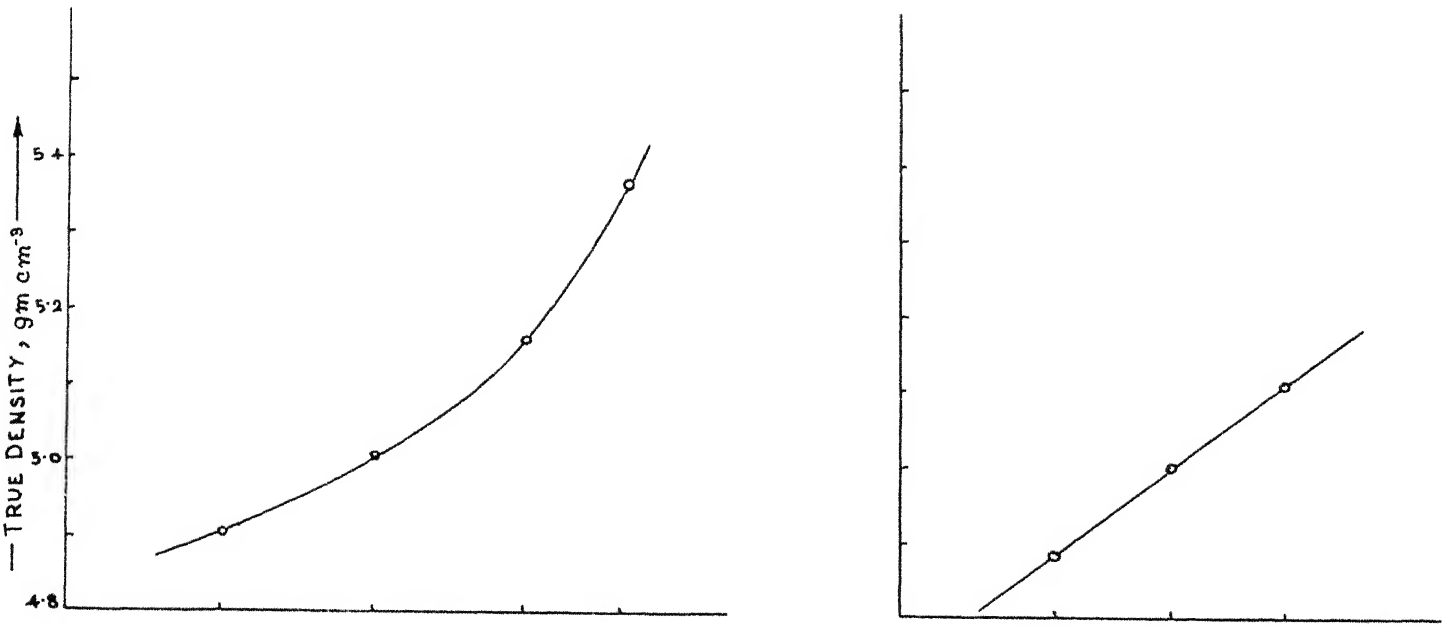

FIG 4·6 TRUE DENSITY VS. COMPOSITION FOR CRUCIBLES.

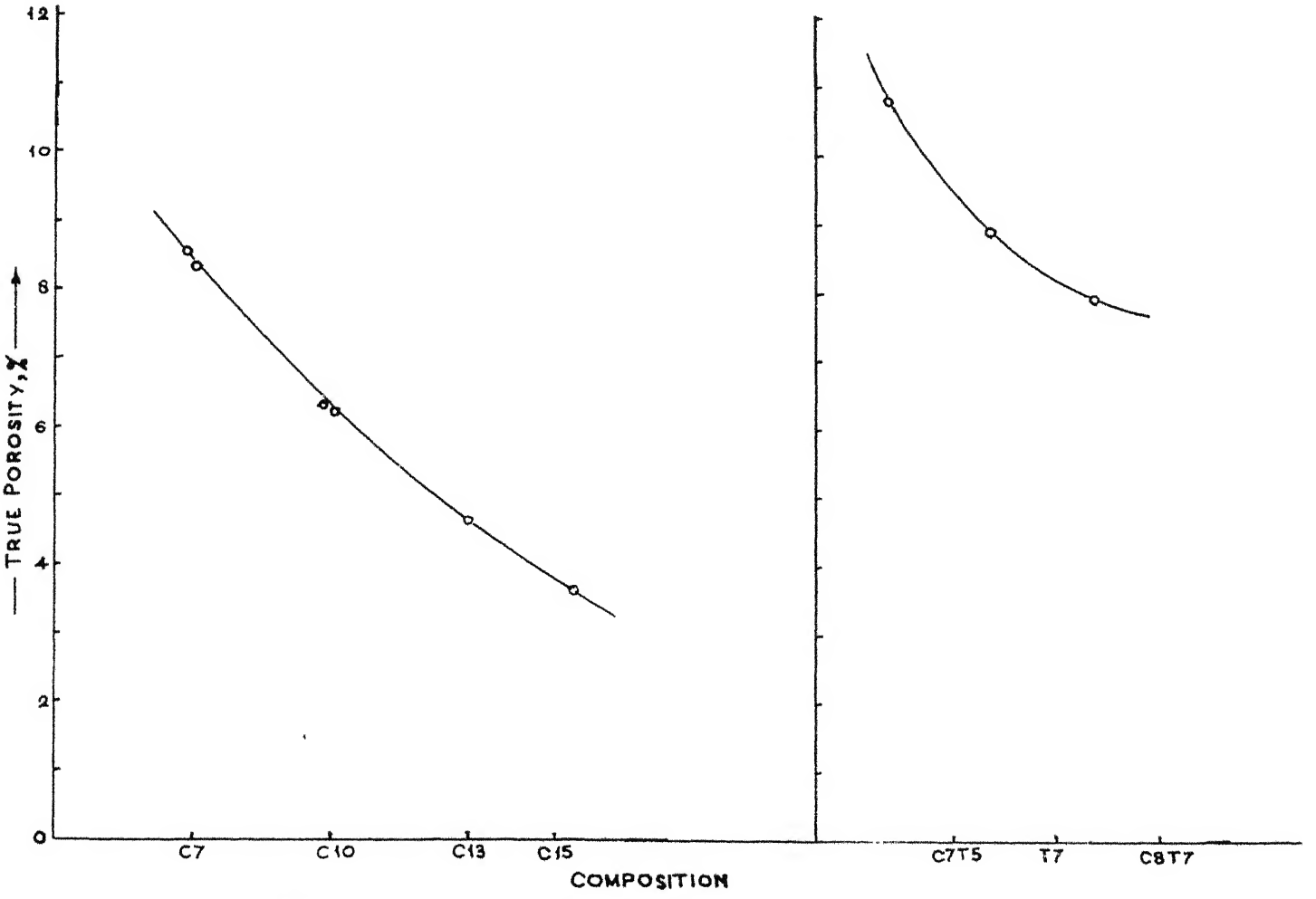

FIG. 4·7 TRUE POROSITY VS. COMPOSITION FOR CRUCIBLES.

closed pores as true porosity is much greater than apparent porosity.

The true porosity ranged between 4.1 for C15 to 13.7 for C7. The M8 batch has a very high porosity 17.65 since it was calcined at 1350°C and on sintering, the samples swelled to some extent.

The porosity figures of $CaO-TiO_2-ZrO_2$ and TiO_2-ZrO_2 batches are much higher than the $CaO-ZrO_2$ compositions. The reason is as follows. Titanium has 4+ valency. So when it will replace Zr^{4+}, no vacancy will be created as opposed to Ca^{2+}. In the latter case vacancies are formed to maintain charge balance. So in case of Ti^{4+} substitution diffusion will be lower than that in the case of Ca^{2+} substitution due to lower number of vacancies in $CaO-TiO_2-ZrO_2$ composition.

Density increased with increasing amount of CaO as more and more liquid phase sintering occured and also at the same time number of vacancies is increased.

Porosity of the crucibles is higher than porosity of the sintered bars because the crucibles were made by slip casting whereby the green density was less than that in the case of pressed bars.

4.2 X-ray Diffraction Studies

The measured 'd' values, respective intensities of the

different lines, integrated intensity and phases present in the sintered samples are shown in tables 4.4a to 4.4i. The X-ray data of the batches after thermal cycling (spalled) are recorded in the tables4.5a-4.5i. The X-ray diffraction curves of sintered and spalled specimens are shown in figure 4.4(i)-(iii) and 4.5 (i)-(iii) respectively.

By comparing the measured 'd' spacings and I/I_o values of our samples with those of ASTM standard we have come to the following conclusion.

The C15 batch contained 95.73% cubic phase and the rest as monoclinic phase, that is the stabilization in this composition was almost complete. In case of C13 batch the cubic phase was only 30.73% indicating the importance of the CaO amount for stabilization. The C10 composition did not get stabilized to the cubic phase. It contained 15.5% tetragonal and 84.5% monoclinic phases respectively.

The C7 composition had only a small amount of tetragonal phase (3.06%) and monoclinic (96.94%) was the major phase. Lower amount of CaO resulted in higher amount of monoclinic form. T7 composition had produced a monoclinic solid solution as indicated by slight change in 'd' values for all (hkl) planes. This agrees with the phase diagram, figure, 2.d. C7T5 batch also formed a single phase monoclinic solid

solution which agrees with the phase diagram, figure 2e. C8T7 composition had developed a small amount of tetragonal phase (5.8%). The M8 batch was also fully monoclinic.

On repeated thermal cycling more and more phase had become ill defined and showed broad X-ray peak and some of them formed humps instead of well defined peaks. This means that the 'd' spacing has been changed, crystallinity has got reduced and micro cracks have been produced throughout the matrix. The C7T5 composition retained some tetragonal phase. It seems that this composition has a low temperature monoclinic-tetragonal phase boundary. The investigation of the phase diagram is necessary in this system to clarify this point.

The composition C7, C10, C13, C15 and Stab Z had also retained tetragonal phase. But retention of tetragonal phase was highest in the two compositions-C7 and C7T5.

On thermal cycling the diffracted intensity from some of the hkl planes increased and the intensity of some of the planes decreased.

The decrease of amount of cubic phase and formation of monoclinic phase is possibly because of the following reason.

At the furnace temperature of thermal shock test the C15 and Stab Z samples got heat treated in the (cubic+monoclinic)

TABLE 4.4

ASTM X-RAY DATA FOR CUBIC, TETRAGONAL AND MONOCLINIC ZIRCONIA

Cubic, a_o = 5.03		Tetragonal, a_o = 5.07, c_o = 5.16	
d Å	I/I_o	d Å	I/I_o
2.96	100	2.93	100
2.56	24	2.52	40
1.81	80	1.81	60
1.54	60	1.79	100
1.48	10	1.55	50
1.28	12	1.53	100
1.17	20	1.47	60
1.04	16	1.29	40
0.98	14	1.27	60
0.90	5	1.17	40
0.86	8	1.13	40
0.85	5	1.10	60
0.81	4	1.05	40
		1.04	70
		0.99	40
		0.98	70

Monoclinic

a_o = 5.1477, b_o = 5.2030,

c_o = 5.3156 β = 99°23'

d Å	I/I_o	d Å	I/I_o
5.036	6	1.656	14
3.690	18	1.640	8
3.630	14	1.608	8
3.157	100	1.591	4
2.834	65	1.581	4
2.617	20	1.541	10
2.598	12	1.508	6
2.538	14	1.495	10
2.488	4	1.476	6
2.328	6	1.447	4
2.285	2	1.420	6
2.252	4	1.358	2
2.213	14	1.348	2
2.182	6	1.321	6
2.015	8	1.309	2
1.989	8	1.298	2
1.845	18	1.269	2
1.818	12	1.261	2
1.801	12		
1.780	6		
1.691	14		

TABLE 4.4

X-RAY DIFFRACTION DATAS OF SINTERED SAMPLES

c = cubic, m = monoclinic, t = tetragonal.

Table 4.4 a. -- Composition C15

2θ degrees	d Å	$\frac{I}{I_O}$	Integrated Intensity	Remarks	% phases
27.2	3.2756	6.0	--	--	--
28.2	3.1617	2.25	4.40	m	4.271
30.26	2.9511	100	158.085	c	95.729
35.08	2.5558	15.02	--	c	--
50.33	1.810	39.04	--	c	--
59.90	1.5428	18.92	--	c	--
62.72	1.4801	5.105	--	c	--

Table 4.4.b.-- Composition C13

2θ degrees	d Å	$\frac{I}{I_o}$	Integrated Intensity	Remarks	% phases
24.2	3.6746	14.35	--	m	--
24.55	3.6230	14.57	--	m	--
28.34	3.1464	100.00	135.98	m	69.27
30.24	2.9530	60.87	96.7	c	30.73
31.58	2.8307	80.44	--	m	--
34.40	2.6048	32.61	--	m	--
35.40	2.5334	30.44	--	m,c	--
38.63	2.3287	7.17	--	m,	--
40.88	2.2055	21.74	--	m	--
45.02	2.0119	11.96	--	m	--
45.62	1.9868	13.48	--	m	--
49.52	1.8391	33.70	--	m	--
50.30	1.8124	65.22	--	m	--
54.16	1.6921	18.26	--	m	--
55.57	1.6521	23.91	--	m	--
60.00	1.5405	38.48	--	m,c	--
62.93	1.4757	24.57	--	m,c	--
64.30	1.4475	8.26	--	m	--
65.80	1.4180	21.09	--	m	--
69.10	1.3582	4.78	--	m	--
71.10	1.3248	13.91	--	m,	--

Table 4.4.c.-Composition C10

2θ degrees	d Å	$\frac{I}{I_o}$	Integrated Intensity	Remarks	% Phases
24.32	3.6567	14.82		m	
24.74	3.5960	9.56		m	
25.63	3.4727	3.46		m	
28.43	3.1367	100.00	145.20	m	84.51
30.41	2.9368	20.43	42.65	t	15.49
31.68	2.8220	58.80		m	
34.33	2.6099	30.15		m	
35.49	2.5272	14.33		t,m	
36.10	2.4859	6.92		m	
38.86	2.3154	8.24		m	
41.08	2.1953	21.90		m	
45.12	2.0051	11.50		m	
45.68	1.9843	14.33		m	
49.48	1.8405	36.57		m	
50.42	1.8084	37.89		t,m	
50.83	1.7945	39.04		t,m	
54.28	1.6885	18.95		m	
55.61	1.6512	44.95		m	
57.41	1.6037	11.04		m	
58.32	1.5808	11.86		m	
60.12	1.5378	28.34		m,t	

Contd...

Contd....C10

2θ degrees	d Å	$\frac{I}{I_o}$	Integrated Intensity	Remarks	% Phases
62.14	1.4925	20.59		m	
62.86	1.4772	16.31		m	
64.60	1.4414	7.91		m	
65.78	1.4184	15.32		m	
71.40	1.3200	14.50		m	
75.40	1.2596	9.89		m	

Table 4.4.d. -- Composition C7

2Θ degrees	d Å	$\frac{I}{I_o}$	Integrated Intensity	Remarks	% phases
24.27	3.6641	13.31	--	m	--
24.68	3.6042	8.40	--	m	--
25.60	3.4767	9.10	--	m	--
28.40	3.1399	100.00	177.52	m	96.936
30.50	2.9283	5.41	8.995	t	3.064
31.63	2.8263	52.80	--	m	--
34.29	2.6126	29.40	--	m	--
35.56	2.5214	10.36	--	t	--
36.00	2.4926	7.28	--	m	--
38.86	2.3154	6.30	--	m	--
40.98	2.2004	21.00	--	m	--
45.02	2.0119	9.38	--	m	--
45.73	1.9823	12.05	--	m	--
49.54	1.8382	35.01	--	m	--
50.42	1.8084	30.80	--	t	--
50.75	1.7974	32.20	--	t	--
54.10	1.6937	21.00	--	m	--
55.63	1.6507	47.48	--	m	--
57.39	1.6043	11.20	--	m	--
58.46	1.5770	13.30	--	m	--
60.23	1.5352	25.21	--	t	--
61.63	1.5037	14.28	--	m	--

Contd....C7

Contd....C7

2θ degrees	d Å	$\frac{I}{I_o}$	Integrated Intensity	Remarks	% phases
62.23	1.4906	20.73	--	m	--
63.02	1.4738	13.59	--	m	--
64.57	1.4420	7.98	--	m	--
65.80	1.4180	13.87	--	m	--
69.37	1.3536	3.92	--	m	--
71.37	1.3205	16.81	--	m	--

Table 4.4.e.-- Composition Stab z

2θ degrees	d Å	$\frac{I}{I_o}$	Integrated Intensity	Remarks	% phases
27.42	3.2499	3.98	--	m	--
28.30	3.1508	2.16	3.5	m	3.036
30.26	2.9530	100.00	179.2	c	96.964
35.11	2.5560	14.10	--	c	--
45.43	1.9947	1.99	--	m	--
50.22	1.8151	43.12	--	m,c	--
59.73	1.5468	5.64	--	c	--
60.22	1.5355	18.24	--	c	--
62.80	1.4782	4.98	--	c	--
74.53	1.2721	2.98	--	m,c	--

Table 4.4.f.-- Composition C7T5

2θ degrees	d Å	$\frac{I}{I_0}$	Integrated Intensity	Remarks	% phases
24.05	3.6971	15.77	--	m	--
24.47	3.6314	10.51	--	m	--
25.29	3.5168	5.12	--	m	--
28.28	3.1529	100.00	--	m	--
31.48	2.8394	56.74	--	m	--
34.12	2.6251	35.04	--	m	--
35.30	2.5400	10.78	--	m	--
35.83	2.5040	7.41	--	m	--
38.60	2.3300	8.63	--	m	--
40.79	2.2154	18.46	--	m	--
44.76	2.0274	11.59	--	m	--
45.48	1.9926	15.50	--	m	--
49.26	1.8489	36.52	--	m	--
50.23	1.8148	32.75	--	m	--
50.57	1.8034	36.12	--	m	--
51.20	1.7827	12.40	--	m	--
54.02	1.6960	15.23	--	m	--
55.41	1.6567	36.79	--	m	--
57.24	1.6081	11.05	--	m	--
58.18	1.5843	15.23	--	m	--

Contd.....

Contd....C7T5

2θ degrees	d Å	$\frac{I}{I_O}$	Integrated Intensity	Remarks	% phases
59.79	1.5454	29.65	--	m	--
61.35	1.5098	14.83	--	m	--
61.93	1.4970	20.22	--	m	--
62.80	1.4784	11.73	--	m	--
64.13	1.4509	5.39	--	m	--
65.63	1.4213	15.23	--	m	--
69.00	1.3599	3.77	--	m	--
71.18	1.3235	13.75	--	m	--

Table 4.4.g. -- Composition C8T7

2θ degrees	d Å	$\frac{I}{I_O}$	Integrated Intensity	Remarks	% phases
24.04	3.6986	18.08	--	m	--
24.63	3.6115	13.56	--	m	--
25.44	3.4982	5.79	--	m	--
28.20	3.1617	100.00	150.875	m	94.215
30.60	2.9190	4.20	5.790	t	5.795
31.48	2.8398	78.48	--	m	--
34.13	2.6259	30.38	--	m	--
35.27	2.5425	14.47	--	m,t	--
38.62	2.3297	10.85	--	m	--

Contd....

Contd....C8T7

2θ degrees	d Å	$\frac{I}{I_0}$	Integrated Intensity	Remarks	% phases
40.77	2.2112	24.77	—	m	—
41.39	2.1796	14.47	—	m	—
44.78	2.0222	12.66	—	m	—
45.55	1.9897	18.08	—	m	—
49.30	1.8468	40.33	—	m	—
50.32	1.8117	48.82	—	m	—
50.50	1.8057	47.92	—	t	—
54.05	1.6951	23.51	—	m	—
55.47	1.6575	37.98	—	m	—
55.94	1.6423	25.32	—	m	—
57.22	1.6060	13.56	—	m	—
58.13	1.5855	16.28	—	m	—
59.93	1.5421	34.72	—	m	—
61.35	1.5098	15.19	—	m	—
61.93	1.4970	16.28	—	m	—
62,90	1.4763	20.43	—	m,t	—
64.34	1.4467	7.41	—	m	—
65.68	1.4204	19.89	—	m	—
69.12	1.3578	6.69	—	m	—
21.21	1.3230	15.37	—	m	—
72.38	1.3045	6.87	—	m	—
75.25	1.2617	12.66	—	m	—

Table 4.4.h. -- Composition T7

2θ degrees	d Å	$\frac{I}{I_0}$	Integrated Intensity	Remarks	% phases
24.27	3.6641	12.41	--	m	--
24.53	3.6113	10.86	--	m	--
25.48	3.4928	3.62	--	m	--
28.30	3.1508	100.00	136.200	m	99.479
30.54	2.9283	0.90	1.143	m	0.521
31.60	2.8289	56.55	--	m	--
34.22	2.6166	22.40	--	m	--
34.43	2.6098	24.48	--	m	--
35.45	2.5300	18.10	--	m	--
38.74	2.3224	9.48	--	m	--
40.95	2.2071	18.97	--	m	--
41.60	2.1691	11.55	--	m	--
44.95	2.0148	9.83	--	m	--
45.91	1.9955	12.41	--	m	--
49.43	1.8422	13.69	--	m	--
50.12	1.8185	36.38	--	m	--
50.63	1.8013	38.45	--	m	--
51.40	1.7762	15.17	--	m	--
54.13	1.6929	15.52	--	m	--
55.54	1.6532	26.38	--	m	--

Contd....T7

Contd....T7

2θ degrees	d Å	$\frac{I}{I_0}$	Integrated Intensity	Remarks	% phases
56.07	1.6388	20.00	--	m	--
57.34	1.6055	14.66	--	m	--
58.38	1.5794	15.86	--	m	--
60.18	1.5364	32.76	--	m	--
61.41	1.5085	10.86	--	m	--
61.90	1.4977	15.00	--	m	--
62.98	1.4746	14.14	--	m	--
64.38	1.4459	6.55	--	m	--
65.79	1.4182	18.45	--	m	--
69.18	1.3568	4.83	--	m	--
71.20	1.3232	12.24	--	m	--
72.85	1.2972	5.17	--	m	--
75.51	1.2580	12.24	--	m	--

Table 4 .4.i. -- Composition M8

2θ degrees	d Å	$\frac{I}{I_o}$	Integrated Intensity	Remarks	% phases
24.05	3.6574	17.17	--	m	--
28.20	3.1617	100.00	--	m	--
31.30	2.8553	51.50	--	m	--
33.99	2.6353	22.22	--	m	--
35.15	2.5509	21.06	--	m	--
38.57	2.3312	8.33	--	m	--
40.78	2.2107	2.50	--	m	--
44.02	2.0204	15.15	--	m	--
45.33	1.9988	18.20	--	m	--
49.11	1.8537	47.98	--	m	--
50.21	1.8155	67.42	--	m	--
53.93	1.6985	17.70	--	m	--
54.33	1.6871	47.22	--	m	--
57.10	1.6117	11.87	--	m	--
58.00	1.5888	15.90	--	m	--
59.92	1.5424	37.52	--	m	--
61.34	1.5100	18.94	--	m	--
61.80	1.4999	23.20	--	m	--
62.60	1.4827	18.94	--	m	--
64.03	1.4529	39.60	--	m	--
65.50	1.3880	20.67	--	m	--
69.01	1.3597	8.33	--	m	--
71.10	1.3248	17.68	--	m	--

TABLE 4.5 X-RAY DIFFRACTION DATAS OF SPALLED SAMPLES

Table 4.5.a. -Composition C15 Spalled

degrees	d Å	$\frac{I}{I_o}$	Integrated Intensity	Remarks	% phases
4.3	3.6596	11.57		m	
4.49	3.6317	11.57		m	
7.29	3.2657	6.25		m	
8.33	3.1473	79.94	112.1	m	53.85
0.30	2.9472	100.00	154.0	c,t	46.15
1.53	2.8350	38.10		m	
4.26	2.6143	37.04		m	
5.30	2.5404	32.87		m	
0.90	2.2045	18.52		m	
4.92	2.0162	16.20		m	
5.65	1.9856	15.74		m	
9.50	1.8398	29.63		m,t	
0.39	1.8094	69.44		m,c,t	
4.13	1.6915	18.75		m	
5.55	1.6529	30.09		m	
7.50	1.6014	16.44		m	
8.40	1.5789	16.44		m	
0.08	1.5387	50.00		m,c,t	
2.94	1.4755	33.10		m	
5.73	1.4194	17.36		m	
1.40	1.3200	12.27		m	
4.59	1.2713	7.18		m,c,t	

Table 4.5.b.- Composition C13 Spalled

2θ degrees	d Å	$\frac{I}{I_o}$	Integrated Intensity	Remarks	% phases
24.4	3.6949	21.67		m	
28.45	3.1345	100.00	65.05	m	87.483
30.42	2.9358	16.67	14.92	c,t	12.517
31.70	2.8202	100.00		m	
34.40	2.6048	32.92		m,t	
35.43	2.5313	22.92		c	
41.07	2.1958	22.50		c,t	
45.03	2.0115	20.83		m	
48.56	1.8732	42.92		m	
50.40	1.8090	62.50		c,m,t	
53.19	1.7205	28.33		t	
55.60	1.6515	37.92		m	
57.53	1.6006	28.33		m	
58.30	1.5813	18.57		t,m	
60.14	1.5373	41.67		c,t,m	
62.68	1.4810	31.20		t,m	
65.90	1.4161	29.17		m	
71.52	1.3181	16.25		t,m	

Table 4.5.c - Composition C10 Spalled

2θ degrees	d Å	$\frac{I}{I_o}$	Integrated Intensity	Remarks	% Phases
24.22	3.6716	16.80		m	
25.60	3.4767	4.56		m	
26.60	3.3982	1.82		m	
28.38	3.1421	100.00	108.575	m	76.64
30.33	2.9402	22.00	53.050	t	23.36
31.57	2.8315	93.41		m	
34.27	2.6137	41.82		m	
35.39	2.5341	25.23		m	
38.72	2.3235	6.82		m	
41.10	2.1943	19.32		m	
41.38	2.1801	17.95		m	
44.92	2.0162	17.95		m	
45.50	1.9918	17.27		m	
49.60	1.8364	42.05		m,t	
50.32	1.8118	55.00		mt,	
54.20	1.6909	29.55		m	
55.60	1.6515	42.95		m	
57.25	1.6078	16.60		m	
58.48	1.5767	15.45		m	
60.13	1.5371	32.05		m	

Contd....C10 spalled

Contd.....C10 Spalled

2θ degrees	d Å	$\frac{I}{I_o}$	Integrated Intensity	Remarks	% Phases
61.40	1.5087	22.73		m	
61.88	1.4982	25.00		m,t	
62.78	1.4809	29.55		m,t	
64.34	1.4467	1.36		m	
65.65	1.4210	22.50		m	
68.87	1.3621	7.50		m,t	
71.20	1.3232	16.14		m	
75.08	1.2641	10.90		m,t	

Table 4.5.d. - Composition C7 Spalled

2θ degrees	d Å	$\frac{I}{I_o}$	Integrated Intensity	Remarks	% Phases
24.23	3.6741	12.22		m	
25.45	3.4969	4.42		m	
28.35	3.1354	100.00	194.03	m	91.741
30.37	2.9406	8.84	28.00	t	8.259
31.60	2.8289	84.83		m	
34.32	2.6107	20.18		m,t	
35.40	2.5334	9.28		m	
38.73	2.3230	3.53		m	
40.92	2.2040	10.31		m	
44.98	2.0136	8.25		m	

Contd...C 7 spalled

Contd....C7 Spalled

2θ degrees	d Å	$\frac{I}{I_o}$	Integrated Intensity	Remarks	% Phases
45.40	1.9959	7.36		m	
49.42	1.8426	18.70		m	
50.30	1.8124	23.86		m,t	
50.87	1.7934	22.09		m	
51.29	1.7797	8.84		m	
52.20	1.7508	2.65		m	
54.14	1.6926	10.01		m	
55.55	1.6526	14.58		m	
57.26	1.6075	7.07		m	
58.39	1.5791	7.36		m,t	
60.12	1.5379	14.43		m,t	
61.46	1.5074	6.19		m	
62.07	1.4940	6.33		m	
62.94	1.4755	8.98		m	
64.50	1.4434	3.53		m	
65.83	1.4369	9.28		m	
71.40	1.3200	4.70		m	
76.23	1.2479	3.40		m	

Table 4.5.e. - Composition Stab Z Spalled

2θ degrees	d Å	$\frac{I}{I_0}$	Integrated Intensity	Remarks	% Phases
24.17	3.6791	4.44		m	
28.31	3.1497	67.80	135.85	m	
30.23	3.9544	79.84	165.17	c,t	
31.50	2.8376	28.40		m	
33.26	2.6914	5.24		m	
34.20	2.6175	29.10		m	
35.22	2.5464	26.98		m,c	
36.86	2.4383	2.86		m	
38.82	2.3177	2.86		m	
40.83	2.2082	9.52		m	
45.57	1.9889	12.60		m	
49.32	1.8461	22.20		m	
50.60	1.8024	100.00		t,c	
53.96	1.6987	7.30		m	
55.57	1.6524	18.40		m	
60.19	1.5362	61.90		t,c	
63.00	1.4742	17.46		m,c,t	
71.35	1.3208	6.98		m	
74.47	1.2730	6.35		m,t,c	

Table 4.5.f.- Composition C7T5 Spalled

2θ degrees	d Å	$\frac{I}{I_0}$	Integrated Intensity	Remarks	% Phases
24.34	3.6527	17.68		m	
28.40	3.1399	100.00	88.93	m	80.779
30.40	2.9377	24.39	33.92	t	19.221
30.95	2.8869	14.33		m	
31.62	2.8272	87.20		m	
34.37	2.6070	47.56		t,m	
35.46	2.5293	24.39		t,m	
38.80	2.3189	6.71		m	
41.00	2.1994	22.87		m	
41.36	2.1811	22.87		m	
45.20	2.0043	21.65		m	
45.62	1.9465	12.20		m	
49.50	1.8398	45.73		t,m	
50.34	1.8110	58.23		m	
50.63	1.8014	58.84		m,t	
54.28	1.6885	30.49		m,t	
55.63	1.6507	50.61		m	
57.27	1.6073	10.37		m	
58.46	1.5772	11.28		m	
60.15	1.5371	36.59		m,t	
61.18	1.5137	18.90		m	

Contd....

Contd.....C7T5 Spalled

2θ degrees	d Å	$\frac{I}{I_o}$	Integrated Intensity	Remarks	% Phases
62.07	1.4940	21.95		m	
63.03	1.4736	18.90		m	
64.53	1.4428	6.71		m	
65.87	1.4361	21.65		m	
71.34	1.3194	19.82		m	

Table 4.5.g. - Composition C8T7 Spalled

2θ degrees	d Å	$\frac{I}{I_o}$	Integrated Intensity	Remarks	% Phases
24.49	3.6317	18.67		m	
25.83	3.4463	5.90		m	
28.62	3.1163	95.82	121.10	m	98.97
30.55	2.9237	3.50	2.06	t	1.03
31.81	2.8107	100.00		m	
34.45	2.6011	39.31		m	
36.62	2.4518	16.71		m	
39.02	2.3063	7.37		m	
41.18	2.1902	25.31		m	
45.12	2.0119	16.22		m	
45.81	1.9791	22.10		m	
46.27	1.9604	4.18		m	

Contd.....

Contd....C8T7 Spalled

2θ degrees	d Å	$\frac{I}{I_O}$	Integrated Intensity	Remarks	% Phases
49.67	1.8340	55.04		m	
50.52	1.8051	56.51		m	
54.34	1.6868	33.91		m	
55.76	1.6472	41.77		m	
57.53	1.6006	20.39		m	
58.40	1.5789	17.69		m	
60.27	1.5343	28.99		m	
61.73	1.5014	16.95		m	
62.15	1.4923	19.66		m	
63.03	1.4736	26.54		m	
64.55	1.4424	11.79		m	
66.11	1.4121	29.48		m	
71.60	1.3167	19.90		m	
72.53	1.3022	12.53		m	

Table 4.5h-- Composition T7 Spalled

egrees	d Å	$\frac{I}{I_o}$	Integrated Intensity	Remarks	% Phases
.24	3.6686	11.67		m	
.58	3.6186	12.92		m	
.43	3.1367	66.67		m	
.60	2.8289	100.00		m	
.28	2.6130	18.54		m	
.57	2.5217	27.50		m	
.82	2.3177	7.50		m	
.21	2.1938	18.75		m	
.98	2.0136	15.83		m	
.78	1.9103	12.71		m	
.50	1.8393	29.17		m	
.51	1.8054	47.08		m	
.32	1.7788	45.00		m	
.73	1.6480	33.33		m	
.23	1.6083	18.33		m	
.12	1.5377	21.04		m	
.59	1.5045	16.04		m	
.12	1.4930	11.25		m	
.11	1.4719	33.33		m	
.99	1.4145	24.38		m	

Contd....T7

Contd. T7 Spalled

2θ degrees	d Å	$\frac{I}{I_o}$	Integrated Intensity	Remarks	% Phases
69.39	1.3532	4.38		m	
71.48	1.3187	7.71		m	
72.79	1.2982	6.25		m	
73.60	1.2859	3.13		m	

Table 4.5.i-Conpositions M8 Spalled

2θ degrees	d Å	$\frac{I}{I_o}$	Integrated Intensity	Remarks	% Phases
24.13	3.6851	14.34		m	
24.51	3.6288	13.44		m	
25.55	3.4834	4.12		m	
28.27	3.1541	100.00		m	
31.55	2.8333	79.75		m	
32.34	2.7658	28.32		m	
35.44	2.5306	19.71		m	
36.87	2.4357	6.81		m	
38.69	2.3253	5.38		m	
40.85	2.2071	19.71		m	
44.98	2.0136	12.00		m	
45.62	1.9868	10.75		m	
49.40	1.8433	23.30		m	
50.40	1.8124	32.26		m	

Contd....M8

td... M8 Spalled

degrees	d Å	$\frac{I}{I_O}$	Integrated Intensity	Remarks	% Phases
.09	1.7235	15.77		m	
.48	1.6549	24.37		m	
.33	1.6057	8.24		m	
.28	1.5818	7.17		m	
.30	1.5336	16.70		m	
.97	1.4748	16.13		m	
.80	1.4180	15.23		m	

phase field. So some amount of tetragonal form was produced which during cooling got transformed to the monoclinic polymorph.

4.3 Microstructure by optical microscopy

Grain size, grain size distribution, porosity, etc. for sintered specimens have been studied by optical microscopy, figures 4.9(i)-4.9(iii)The average grain size for the batches C7, C10, C13, C15 & Stab Z are 14.3 , 7.2 , 10, 13.9 , 18.6 microns respectively. It has been found that except for the batch C7, the grain sizes of the other calcia-zirconia batches have increased with increasing CaO content. This can be explained by the increased diffusion rate due to larger number of vacancies for higher CaO-containing batches. Though the grain size of the C7 batch is high, yet there are enough intergranular and intragranular pores to make the density low. With the addition of TiO_2 to $CaO-ZrO_2$, grain size has decreased as C7T5 batch has an average grain size of 11.4 micron and for C8T7 batch the grain size is 4.3. micron. The reason lies in the lower diffusion rate due to lower vacancy concentration.

4.4 Vickers Hardness

Vickers hardness numbers(VHN) are shown in table 4.6 and fig. 4.10. It has been found that for $CaO-ZrO_2$ systems

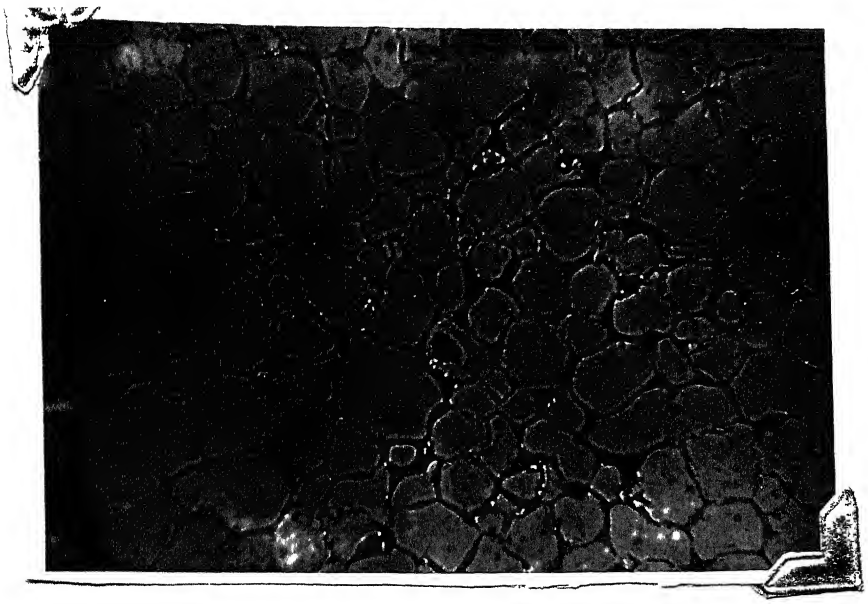

Fig. 4B (N1) M8
200×

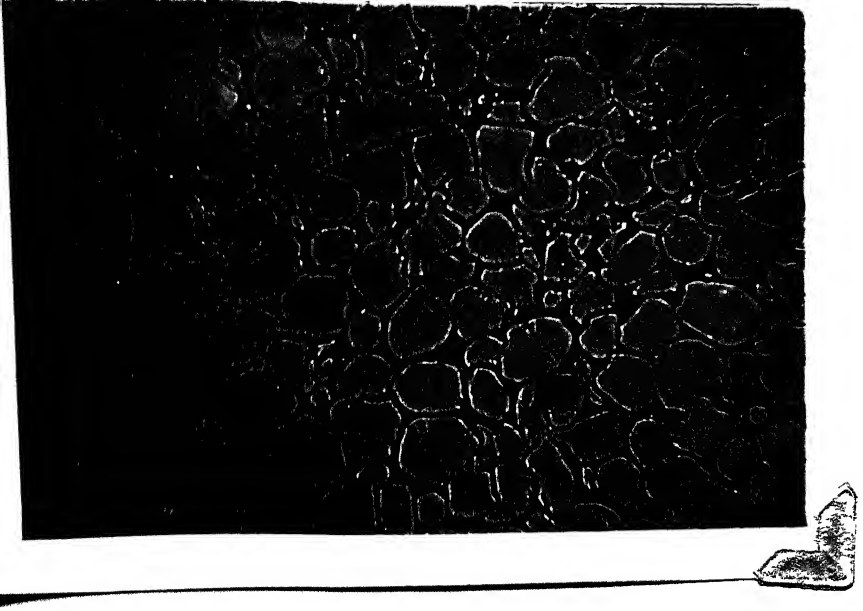

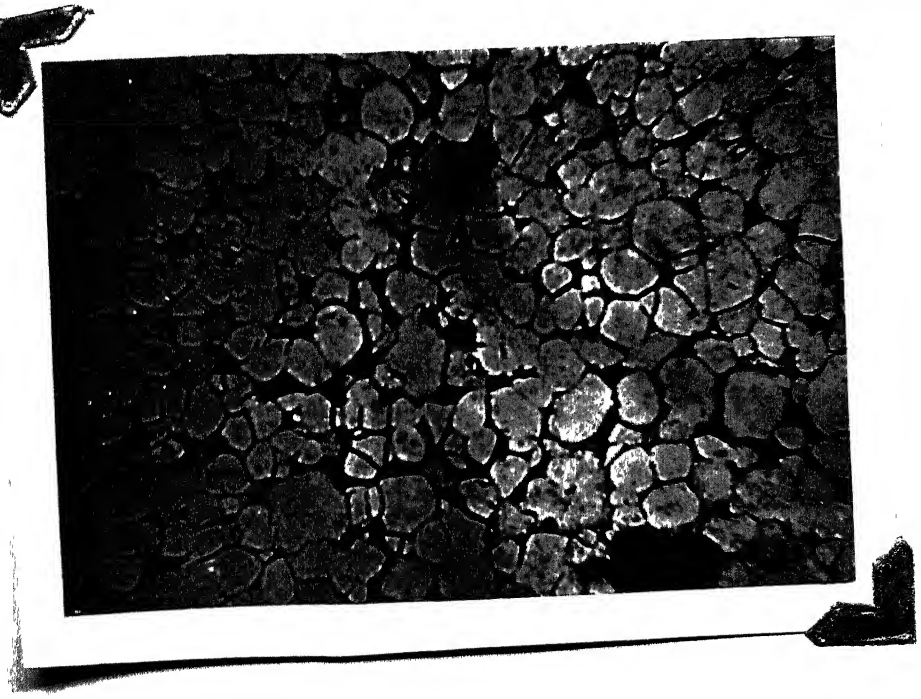

TABLE 4.6

VICKERS HARDNESS & INDENTATION CRACK LENGTHS

Compositon	Load in Kg	Length of diagonal x 10^{-3} mm	Crack length x 10^{-3} mm	VHN
1	2	3	4	5
Stab Z	2.5	63	94	1168
	2.5	56	71	1478
	2.5	55	63	1533
	5.0	82	95	1379
	5.0	86	54	1253
C10	2.5	90	No crack	572
	2.5	69	"	974
	2.5	83	"	673
	2.5	91	"	560
	5.0	126	25	584
C13	2:5	75	No crack	824
	2.5	85	"	641
	2.5	73	"	871
	2.5	70	"	946
	2.5	70	"	946
	5.0	123	18	613

Contd...

Contd....4.6

1	2	3	4	5
C15	2.5	75	86	824
	2.5	75	93	824
	2.5	79	147	743
	2.5	69	167	976
	5.0	129	55	558
	5.0	133	79	613
C7T5	2.5	86	No crack	626
	2.5	88	"	598
	2.5	82	"	689
	2.5	88	13,Very thin crack	598
	5.0	125	No crack	595
C8T7	2.5	81	No crack	706
	2.5	86	"	626
	2.5	82	"	689
	2.5	85	"	641
	2.5	82	"	689
	5.0	126	16	593
	5.0	114	14	713

Contd....4.6

Contd... 4.6

1	2	3	4	5
C7	2.5	87	No crack	612
	2.5	91	13	560
	2.5	73	18	870
	2.5	90	23	572
	5.0	145	No crack	441
T7	2.5	100	18	463
	2.5	93	12	536
	2.5	92	13	547
	2.5	93	15	536
	5.0	140	83	473
	5.0	288	30	112
	5.0	181	13	283

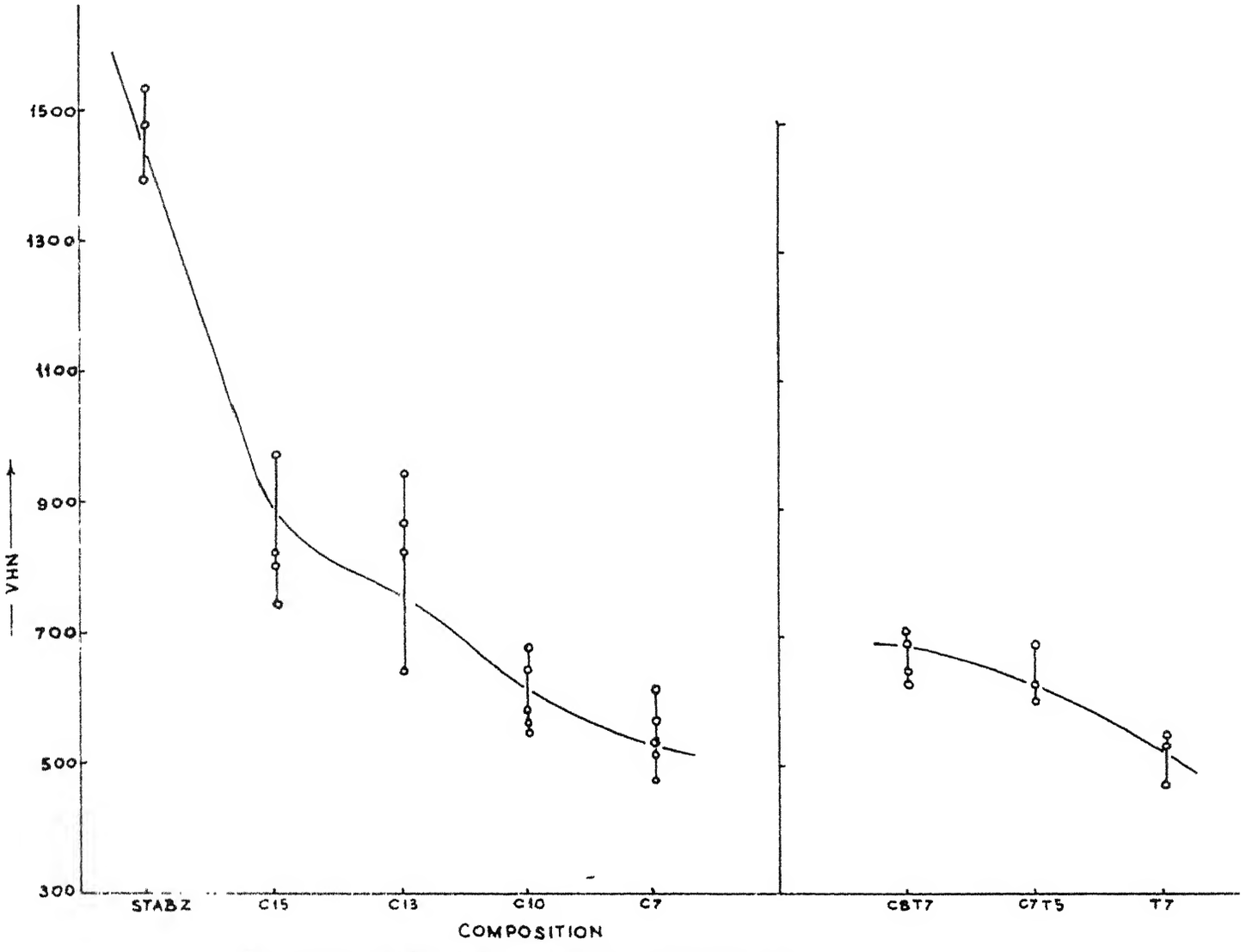

FIG 4·10 VICKERS HARDNESS NO VS. COMPOSITION

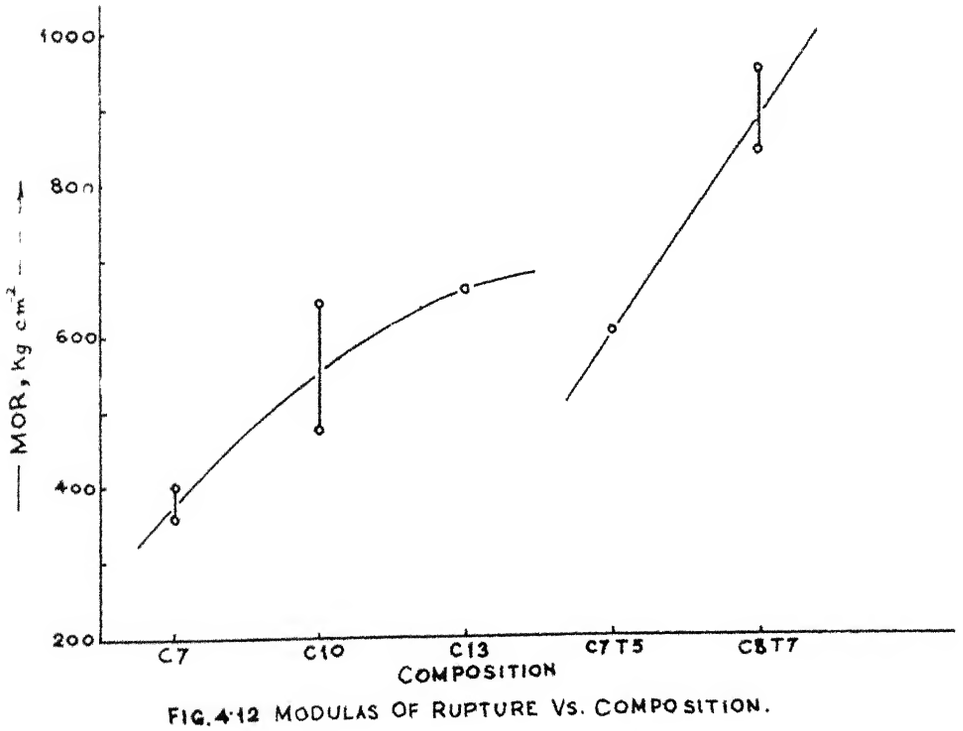

FIG. 4·12 MODULAS OF RUPTURE VS. COMPOSITION.

VHN has increased with increase of CaO content which is natural as the higher CaO containing batches are of higher density. For the $CaO-TiO_2-ZrO_2$ batches the trend is similar i.e., with increase of density the VHN has increased.

4.5 Fracture toughness

The fracture toughness values of different batches as determined by indentation technique are shown in table 4.7. The values were obtained by first estimating the quantity

$$\frac{\phi}{H\sqrt{a}}\left[\frac{H}{\phi E}\right]^{0.4}$$

by using Young's modulus E $\simeq$155.7 GN/m^2 for C7, C10, C8T7, C7T5 and T7, 80 GN/m^2 for C13 and 67.53 GN/m^2 for C15 and Stab Z (35). The constraint factor was taken as 3 (34). Hardness, H was obtained from equation 3.12 (33) using the experimental values of impression radius a . The dimensionless parameter $K_c\phi\left[\frac{H}{\phi E}\right]^{0.4}$ was obtained from the calibration curve (13, 34) by using the experimentally obtained values of $\frac{c}{a}$. The ratio of the two quantities yielded the magnitude of k_c. All the experimentally obtained and calculated parameters are shown in table 4.7.

The C15 composition has the lowest fracture toughness, Stab Z has similar value. The fracture toughness values of C7, C10, C13 are much higher than those of C15 and Stab Z

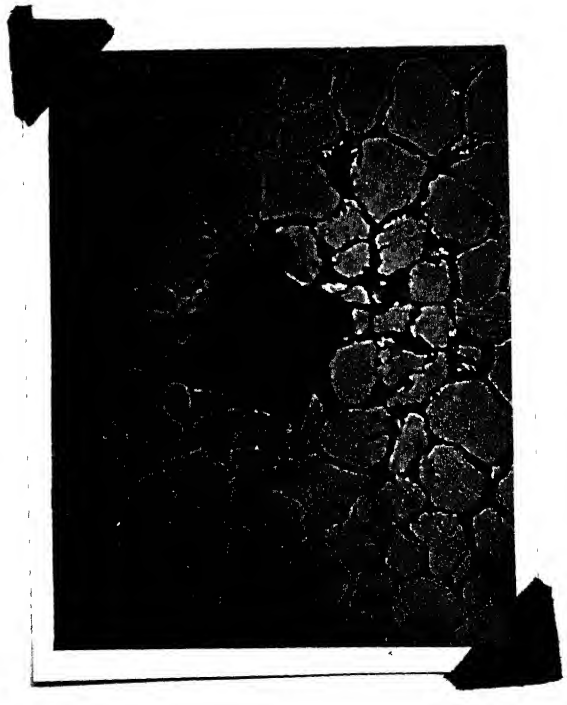

Fig. 4.11. (Wild)
C/T 7
200X
5 Kg load

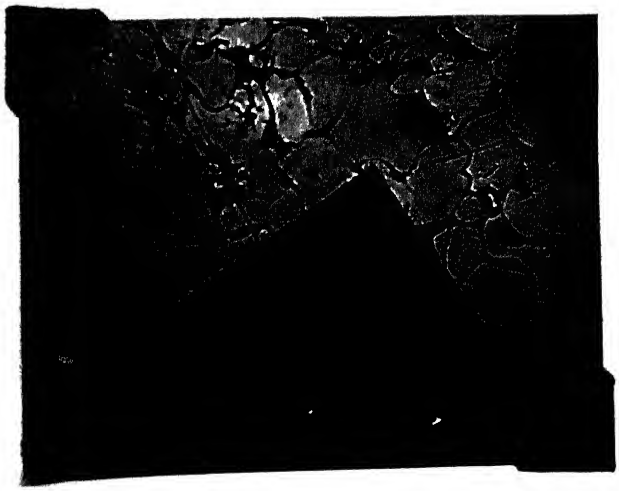

Fig. 4.11. (Wild)
CET7
200X
5 Kg load

TABLE 4.7

FRACTURE TOUGHNESS

Composition	Impression radius $a \times 10^{-6}$ m	Average crack length $\bar{C} \times 10^{-6}$ m	$\frac{\bar{C}}{a}$ dimensionless	H GNm^{-2}	E GNm^{-2}	$\phi(\frac{H}{E})^{0.4}$ $GN^{-1}m^{3/2}$	$k_c\phi(\frac{H}{E})^{0.4}\frac{\bar{C}}{a}$ dimensionless	K_C $MNm^{-3/2}$
1	2	3	4	5	6	7	8	9
Stab Z	86	54.5	0.6337	14.484	67.53	9.7666×10^{-3}	0.0540	5.527
	56	71.0	1.267			9.6349×10^{-3}	0.0452	4.691
	55	63.0	1.146			9.7220×10^{-3}	0.0471	4.840
C15	75	93.0	1.240			1.163×10^{-2}	0.0455	3.912
	75	86.0	1.147	8.295	67.53	1.1630×10^{-2}	0.0471	4.045
	79	147.0	1.861			1.1333×10^{-2}	0.0371	3.269
	128	78.0	0.609			8.9033×10^{-3}	0.0553	6.205
C13	123	18.0	0.1463	8.075	80.00	6.6087×10^{-3}	0.0590	8.626
C10	126	25.0	0.1984	6.142	155.7	6.529×10^{-3}	0.0593	7.691
C7	91	13.0	0.143			9.840×10^{-3}	0.0598	6.072
	145	5.0	0.007	5.367	155.7	7.80×10^{-3}	0.0607	8.076
	90	23.0	0.256			9.87×10^{-3}	0.063	5.997

Contd....

1	2	3	4	5	6	7	8	9
C8T7	126	16	0.127	6.755	155.7	7.2677×10^{-3}	0.0602	8.290
	114	14	0.123			7.6406×10^{-3}	0.0603	7.893
C7T5	86	1	0.023	6.142	155.7	9.3137×10^{-3}	0.0622	6.678
	82	1	0.012			9.538×10^{-3}	0.0622	6.521
T7	140	53	0.3786	5.252	155.7	8.0186×10^{-3}	0.0575	7.172
	181	13	0.0718			7.0522×10^{-3}	0.0617	8.749
	93	12	0.129			9.8380×10^{-3}	0.0602	6.119
	100	18	0.18			9.488×10^{-3}	0.0598	6.303
	92	13	0.1413			9.892×10^{-3}	0.0597	6.040
M8	383	110	0.287	5.4	155.7	4.7678×10^{-3}	0.0379	7.949
	218	146	0.6697			6.3196×10^{-3}	0.0468	7.406
	209	149	0.713			6.4543×10^{-3}	0.0458	7.096

as shown in the table.

With addition of TiO_2, in all the cases, the fracture toughness values have increased. T7 has the highest fracture toughness. C7T5 and C8T7 are also good in respect of fracture toughness.

In C7, C10, and C13 batches the major phase is monoclinic and the rest is tetragonal for C7, C10 and cubic for C13. But C15 and Stab Z are nearly single phase cubic zirconia. It isawell known fact that the fracture toughness value of cubic ZrO_2 is low which explains the lower fracture toughness of C15 and Stab Z batches.

form

C7T5, T7 and M8 batches/fully monoclinic solid solutions on sintering. C8T7 in addition to being a monoclinic SS, contains a small amount of tetrogonal ZrO_2.

The tougher materials at the same time are of low hardness value. This can be explained from the equation number 3.10. Lower hardness means higher indentation impression radius (a) and consequently higher K_c or in other words higher toughness.

The low fracture toughness value in C15 and Stab Z is evident from the figure (4.11a-i) showing the indentations surrounded by many big cracks even with 2.5 Kg load. Indentation in T7 developed small cracks with 2.5 kg load. Rest of the

batches did not show any crack at 2.5 kg load. The later batches excepting C7 however developed small cracks at 5 kg load.

Finally, it will be worthwhile to mention here that our fracture toughness values are comparable or even better than the values obtained by other workers. This has been shown in table numbers (4.7 & 4.8).

TABLE 4.8

FRACTURE TOUGHNESS VALUES OF DIFFERENT MATERIALS

Composition	K_C MN $m^{-3/2}$	Reference
Mgpsz	2-6	Porter and Hener (12-22)
Y_2O_3-psz	6-9	Gupta, Lange etal (13)
BC	6	Evans & Charles (32)
Saphire	2.1	" "
Spinel	1.31	" "
Si_3N_4	4.9	" "
SiC	4	" "

Table 4.9 Modulus of rupture

mposition	Thickness of the sample d,mm	Width of the sample b,mm	Load, Kg	MOR $Kg/cm.^2$	MOR, $x10^3$ psi
T5	8.2	5.62	30	608.13	8.65
T7	7.9	5.46	42.9	956.33	13.6
				843.27	11.99
				847.65	12.10
3	7.92	5.60	31.3	661.60	9.41
O	8.54	6.60	45.50	642.13	9.13
				473.30	6.73
	8.95	6.00	12.60	400.24	5.69
				356.92	5.07
	9.83	5.98	31.7	473.44	6.73
				736.06	10.47

4.6 Modulus of Rupture (MOR)

MOR values are recorded in table 4.9 and the variation of MOR with composition is shown in the figure 4.12. It is evident from the table that with addition of TiO_2 the MOR value has increased. As for example, the MOR value of C7 batch is nearly 375. Kg/cm^2 and for C7T5, it is 608 Kg/cm^2. One of the possible reasons is the higher density of the TiO_2 added batches. The other reason may be in higher toughness value in TiO_2 containing batches.

4.7 Thermal Shock Resistance

Thermal shock resistance is measured by the number of thermal cycles excluding the last cycle, the last cycle being defined by the chipping, or crumbling of the samples, or pulling apart by tongs. Figure 4.13 shows the number of cycles before failure as a function of composition. This figure gives an obvious trend of decreasing spalling resistance from C7T5 to C15 in the following order

C7T5 > M8 > C7 > C8T7 > C10 > T7 > Stab Z > C13 > C15.

The C13, C15 and Stab Z batches contain higher percentage of cubic phase and have much lesser thermal shock resistance than the others. The C7T5 batch has the highest thermal shock resistance.

TABLE 4.10

THERMAL SHOCK RESISTANCE

Batch	No. of Cycles before failure	Batch	No. of Cycles before failure
C7	16	C7T5	23
C7	11	C7T5	15
C10	12	C8T7	14
C10	8	C8T7	9
C13	4	M8	18
C13	5	M8	14
C15	5	M8	14
C15	5	T7	12
C15	8	T7	8
C15	3	T7	8
C15	1	Stab z bushing	10
C15	2		
C15	3	Stab z bushing	11
		Stab z bushing	8

C7T5 > M8 > C7 > C8T7 > C10 > T7 > Stab z > C13 > C15

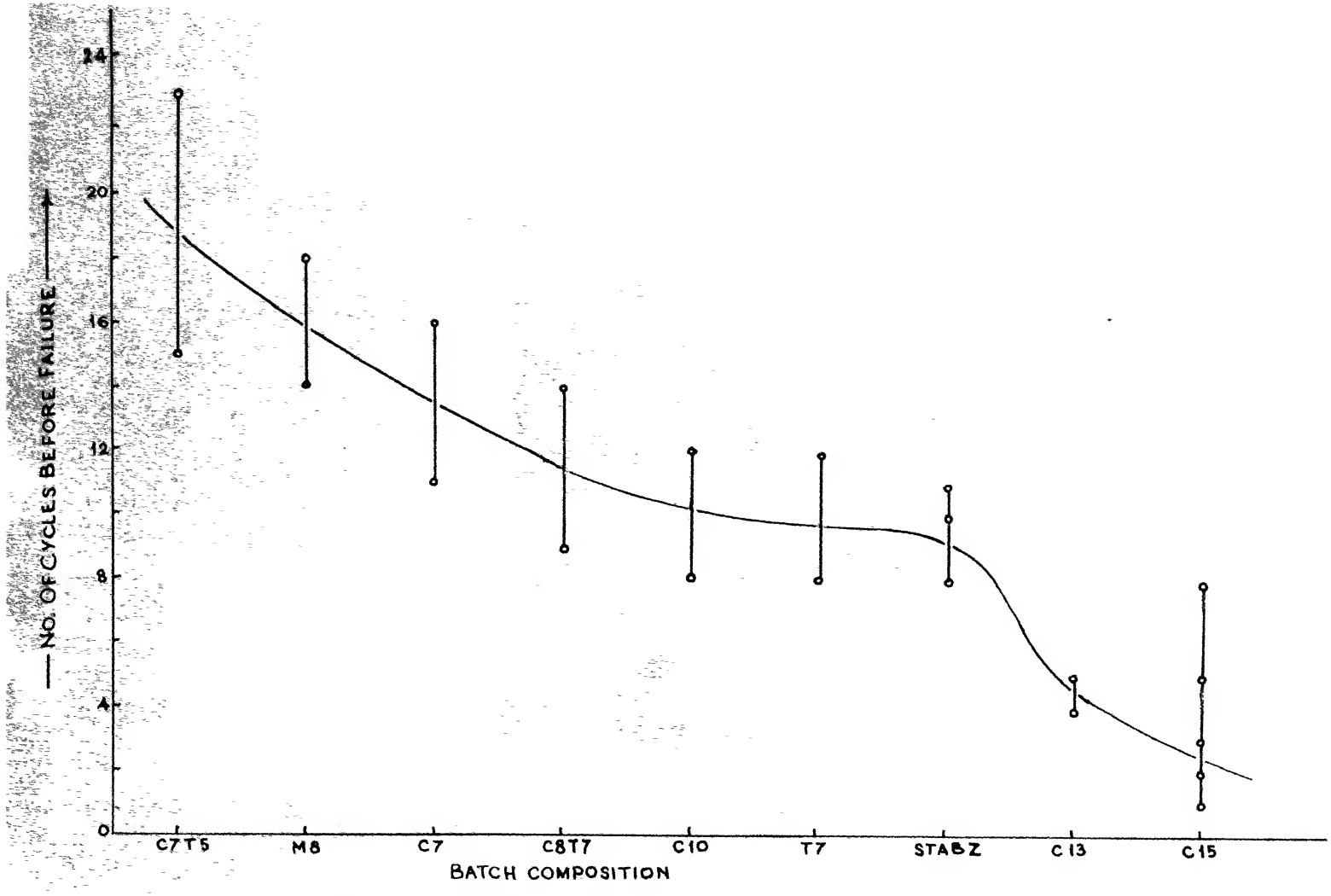

THERMAL SHOCK RESISTANCE VS. COMPOSITION

Thermal shock resistance (spalling resistance) is a property which is dependent on many factors namely thermal conductivity, thermal expansion coefficient, temperature gradient, grain size, grain size distribution, pore size, pore size distribution, presence of glassy phase, type of phase of ZrO_2, etc. So more detailed work is required to find out the possible reasons of the above trend in thermal shock resistance.

4.8 Corrosion resistance

The corrosion resistance of the zirconia crucibles in contact with E glass has been found to be good. The crucibles containing the E glass in the corrosion resistance test did not get affected, except only a little thinning at the air-glass-ZrO_2 interface for some batches. TiO_2 containing batches also showed similar corrosion resistance properties. The interface corrosion is the least in C7 crucibles. Next is M8 crucible. But corrosion in the bulk is not observable in any of the batches. In contrast, the Al_2O_3 crucible has got heavily corroded; Corrosion at the air-glass Al_2O_3 interface is more pronounced than in the interior. In case of Al_2O_3, a layer of intermediate compositions between Al_2O_3 and glass has formed by dissolution of Al_2O_3 which rendered it visible. The photographs of the crucibles after corrosion resistance test are shown in fig. 4.14.

4.9 Discussions on experimental procedure

4.9.1 Grinding

Grinding was done in alumina lined ball mill and agate ball mill. In order to avoid extraneous contamination from the jar and balls ; grinding could be done in steel jars using steel balls; and then the incoming iron has to be removed by magnetic separation. Longer grinding of C8T7 and C7T5 batches did not produce remarkable effect on the particle size distribution as compared to $CaO-ZrO_2$ batches because of the fact that these two batches got calcined to a greater strength than the others. So, in general, C8T7, C7T5 batches seem to need longer grinding.

4.9.2 Pressing

A moderately high pressure was used. Very high pressure causes steep pressure gradient contours.

4.9.3 Sintering

We used 1 hour soaking period at 1950°C, but longer period can be used for higher sintered density. More work is required to optimise the soaking period & temperature.

The zirconia batches should be tried for further heat treatments of solution annealing at 1800-1900°C for dissolving the monoclinic phase, quenching to 1000°C followed by ageing

etween 1250 to 1350°C and finally slow cooling. This may ead to retention of more tetragonal phase.

4.9.4 X-ray diffraction study

It was done with as sintered bars, It was not ground to powder as grinding and mechanical stresses trigger tetragonal-monoclinic phase transformation and leads to wrong idea about the tetragonal phase (22, 24) by X-ray diffraction.

4.9.5 Thermal shock resistance

According to ISI Specification (36), the temperature used for thermal cycling to measure the thermal shock resistance for SiO_2 bricks is 450°C, and that for fire brick, siliceous and basic bricks, is 1000°C. Since ZrO_2 has much higher melting temperature (2690°C), so we have used 1300°C for thermal cycling.

4.9.6 Corrosion resistance.

More work is required to establish the corrosion resistance property of our samples. We have studied the corrosion resistance of our samples in contact with E glass (which is more corrosive than A, C, S and HS glasses). But corrosive effects of other glasses and slags are to be tested. At the same time, long duration corrosion resistance tests are also necessary to characterize these materials properly.

4.9.7 Mechanical Properties

Though we have measured MOR, VHN and Kc, but young's modulus in tension should also be measured for better characterization of our materials.

CHAPTER 5

CONCLUSION

1. The average particle size of the powder ($\sim$ 0.2 micron) which we used for final sintering is optimum size, because higher particle size means settling of the slip used for slip casting and less densification and finer particles will give rise to drying cracks after casting.

2. With addition of TiO_2 in CaO-ZrO_2 systems, the bulk density has decreased at the cost of improvement of other properties.

3. In all the TiO_2 containing batches, the major phase is monoclinic, no cubic phase (ZrO_2) is formed. In C8T7, small amount of tetragonal phase is formed, whereas cubic phase is present in C13 and C15 batches, but no tetragonal phase has been found.

4. Grain size can be controlled to some extent by adding TiO_2. Finest grain size has been obtained in C8T7 composition.

5. With addition of CaO, the hardness (VHN) has increased in all the cases, the same is true for TiO_2 addition but the increase in hardness is not so appreciable.

6. For the same amount of CaO, MOR values have been increased on addition of TiO_2. Maximum MOR has been obtained for C8T7 composition.

composition.

7. Fracture toughness values are good for all the compositions except C15 and Stab Z. TiO_2 addition has increased the fracture toughness to a small extent.

8. Spalling resistance is maximum for the composition C7T5, followed by M8. C15 has the lowest thermal shock resistance. So TiO_2 has good effect from thermal shock point of view.

9. Corrosion resistance of C7 composition is highest, the next is M8. Corrosion resistance of TiO_2 - added samples are comparable to those of CaO-added crucibles though not better than CaO-added crucibles.

10. So, finally, it can be said that C7T5 and C7 compositions can be advocated for ZrO_2 bushing for glass fiber drawing from both mechanical and thermal characteristics and corrosion resistance point of view.

REFERENCES

1. Special Ceramics, 1960.
2. R.H.J. Hannink, Growth morphology of the tetragonal phase in psz. J. Maths. Sc. 13 (1978) 2487-2496.
3. M.L. Mishra, Refractories, 1975.
4. A.V. Seybolt and Burke, Procedures in Experimental Metallurgy.
5. S.P. Reddy & G. Mandal, Some aspects of production and uses of zirconia and its indegeneous raw material resources. Trans. Ind. Cer. Soc. V35 (5) 1976 P35 N.
6. K.C. Redford & R.J. Bratton. Zirconia electrolyte cell, J. Matls. Sc. 14 (1979) 59-65.
7. D. Chakravorty et.al. Unpublished results.
8. G.V. Bansal and A.H. Heuer, On a martensitic phase transformation in zirconia - 1. Metallographic evidence. Acta Metallurgica - 20 (1972) 1281-1289.
9. E. Ryskhewitch, Oxide Ceramics, 1960, Academic Press.
10. Salmang-Ceramics-Physical & Chemical fundamentals. 1961, Butter Worths.
11. T.K. Gupta, J.H. Bechtold, et.al. Stabilization of tetragonal phase in polycrystalline ZrO_2. J. Matls. Sc. 12 (1977) 2421-2426.
12. D.L. Porter & A.H. Heuer, Mechanism of toughening in psz, J. Amer. Cer. Soc. V60, N3-4, 1977, 183.
13. T.K. Gupta, F.F. Lange, J.H. Bechtold, Effect of stress induced phase transformation on the properties of polycrystalline ZrO_2 containing metastable tetragonal phase. J. Matls. Sc. 13 (1978) 1464-1470.

14. G.K. Bansal, A.H. Heuer, Precipitation in partially stabilized zirconia. J. Amer. Cer. Soc. 58 (5-6) 235 -238 (1975).

15. R.C. Garvie & P.S. Nicholson, Structure and Thermo-mechanical properties of psz in the CaO-ZrO_2 system. ibid, V55, N3 (1972), 152.

16. R.C. Garvie, R.H. Haunink & R.T. Praseo, ceramic steel? Nature 258 (1975) 703.

17. Nils Claussen, Comments on precipitation in psz. J. Amer. Cer. Soc. V.59, 3-4 (1976) 179.

18. D.L. Porter, G.K. Bansal & A.H. Heuer, ibid V59, N 3-4, (1976) 179-182.

19. D.L. Porter, A.H. Heuer, Reply to discussion in psz. ibid., V60, N 5-6, (1977) 280-281.

20. Roy, W. Rice. Further discussion on precipitation in psz. ibid V60, N 5-6 (1977) 280-281.

21. Nils Claussen, Stress induced transformation of tetragonal ZrO_2 particles in ceramic materials. ibid, V61, N 1-2, 85-88 (1978).

22. D.L. Porter and A.H. Heuer. Microstructural development in MgO psz. ibid V62, N 5-6, (1979) 298-305.

23. A.H. Heuer. Application of TEM to Engineering particle in ceramics. ibid. V62, N 5-6 (1979) 226-235.

24. T.K. Gupta, Strengthening by surface damage in Metastable Tetragonal zirconia. ibid, V63, N 1-2 (1980 117.

25. F.F. Lauge, Technical Report No. 2, Stress Induced Martensitic Reaction : I Theory of metastable phase retention and contribution to fracture toughness. July 1978.

26. F.F. Lange, T.R. No. 3. Stress Induced Martensitic Reaction: II Experiments in the ZrO_2-Y_2O_3 system., July 1978.

27. Paul H. Rieth, J.S. Reed & A.W. Nauman. Fabrication and flexural strength of ultrafine grained Y_2O_3-stabilized ZrO_2. Amer. Cer. S. Bulletin. V55, N8, 717 (1976).

28. A.M. Alper, High temperature oxides. 1971.

29. Levin, Phase diagrams for ceramists.

30. Van Vlack, Materials Science for Engineers, 1971, Addison Wiley.

31. ISI Specification, 1528 parts VIII and IX.

32. Grimshow. The Chemistry and Physics of clays and allied ceramic materials, 1971, Earnest Benn Ltd.,

33. Dieter, G.E., Mechanical Metallurgy, MC Grawhill, 1961.

34. Evans, A.G. and Charles, E.A. Fracture toughness determination by indentation, J. Amer. Cer. Soc., 59 (1976) 371.

35. Engineering Properties of Ceramic materials. Amer. Cer. Soc. 1966.

36. ISI Specification : IS 1528, Part III.